NASA Contractor Report 4553

Nonintrusive Fast Response Oxygen Monitoring System for High Temperature Flows

Daniel B. Oh and Alan C. Stanton
Southwest Sciences, Inc.
Santa Fe, New Mexico

Prepared for
Langley Research Center
under Contract NAS1-19097

National Aeronautics and
Space Administration
Office of Management
Scientific and Technical
Information Program
1993

PAGE _____ INTENTIONALLY BLANK

PROJECT SUMMARY

The monitoring and control of molecular oxygen concentrations is important in the operation of high temperature wind tunnels used in development and testing of hypersonic air-breathing engines. Maintaining proper O_2 concentrations is important to avoid damage to test engines and to permit accurate studies of engine performance. Fast time response in monitoring and control of O_2 is required, since the run time of large wind tunnels is often less than one minute. Also, experimental research on airbreathing hypersonic propulsion requires new diagnostic capabilities for nonintrusive measurement of important flow and engine performance parameters (e.g. inlet mass capture, combustion efficiency, thrust). Nonintrusive measurement of species concentrations, gas temperature, and flow velocity can provide much of the needed information. The purpose of this study is to investigate a new concept for nonintrusive, fast-response measurement of O_2 number density and other flow parameters in high speed wind tunnels, based on absorption of near-infrared radiation from inexpensive commercial laser diodes used in the optoelectronics industry.

In the Phase I research, laboratory breadboard instrumentation incorporating a standard commercial GaAlAs diode laser was used to measure molecular oxygen in room air, in air heated by a tube furnace at 1375 K, and in a methane-oxygen flame. The technique of high frequency laser modulation with harmonic detection was used to obtain very high sensitivity for measurement of small optical absorptions. In addition, the use of fiber optics in O_2 monitoring instrumentation based on this technique was investigated.

The primary goals of the Phase II research and development program have been to implement this diagnostic approach in prototype instrumentation that can be used for nonintrusive *in situ* measurement of O_2 concentration, gas temperature, and flow velocity in wind tunnel facilities at the NASA Langley Research Center. The instrumentation is designed for simultaneous measurements along multiple lines of sight accessed by fiber optics. Molecular oxygen concentration is measured from the magnitude of absorption signals, gas temperature (rotational temperature) is determined from the intensity ratio of two O_2 absorption lines, and flow velocity is measured from the Doppler shift of absorption line positions.

The prototype instrument has been tested extensively in laboratory flames, emphasizing assessment of the instrument's capabilities for quantitative measurement of O_2 concentration (mole fraction) and gas temperature. Fuel-lean premixed methane/O_2 flames were studied, using a flat flame burner. The spectroscopically determined temperatures were found to be in generally good agreement with thermocouple measurements, while the spectroscopically derived values for O_2 mole fraction were found to be systematically lower than the values expected from flame stoichiometry. This latter result is shown to be a consequence of nonuniform temperature profiles across the line of sight, particularly the cooler edges of the flame. Careful selection of the O_2 absorption line(s) used for concentration measurements, based on approximate knowledge of the temperature field, can minimize the systematic errors due to

nonuniform temperature. The specific absorption lines used in this work are expected to be well suited to measurements in systems with gas temperatures in the 600 to 1000 K range, but a different choice of lines may be indicated for higher or lower temperature flows.

The detection sensitivity in the flame experiments corresponds to a minimum detectable absorbance of about 4×10^{-6} at detection bandwidths of about 1 Hz. This sensitivity is achieved only by subtraction of background interference fringes due to scattering from various optical surfaces in the fiber optic system, especially the input and output coupling optics. At least an order of magnitude improvement in sensitivity has been achieved when the fiber optics are removed from the system and the number of transmissive optical components is minimized.

The near-infrared diode laser absorption techniques studied in this program may also be applied to the measurement of other important gases in combustion, such as fuel or product species. Water vapor is a natural candidate species that is important in hypersonic combustion and can be measured with high sensitivity using near-IR InGaAsP lasers. Other potential applications of this technology include toxic or contaminant gas detection, on-line monitoring of industrial processes, pollutant monitoring, and atmospheric research.

TABLE OF CONTENTS

1. INTRODUCTION

Successful development of hypersonic airbreathing propulsion for missions such as the National Aero-Space Plane requires new diagnostic capabilities for nonintrusive measurement of important flow and engine performance parameters. For example, combustion efficiency could be determined from *in situ* measurements of molecular oxygen or water vapor concentrations or other important combustion species at the combustor exit. Inlet mass capture could be determined from simultaneous measurements of density and velocity at the inlet. In related applications, real-time monitoring and control of oxygen concentrations is important in high temperature wind tunnels operating with vitiated air to avoid damage to test engines and to allow accurate studies of engine performance. Fast time response in diagnostic systems designed to address these needs is required, since the run time of hypersonic wind tunnels or other engine test facilities is often less than one minute.

The purpose of this study is to develop and apply a new idea for nonintrusive measurement of O_2 in supersonic combustion studies, based on absorption of near-infrared radiation from inexpensive commercial laser diodes used in the optoelectronics industry. In Phase I of this research, laboratory breadboard instrumentation incorporating a standard commercial GaAlAs diode laser was used to measure molecular oxygen in room air, in air heated by a tube furnace at 1375 K, and in a methane-oxygen flame. The technique of high frequency laser modulation with harmonic detection was used to obtain very high sensitivity for measurement of small optical absorptions. In addition, the use of fiber optics in O_2 monitoring instrumentation based on this technique was investigated.

The primary goal of the Phase II research and development program is to implement this nonintrusive diagnostic technique in test facilities at the NASA Langley Research Center. Several important technical issues are addressed in Phase II. These issues include adapting the technique for simultaneous measurements in multiple optical channels accessed by fiber optics. Techniques for quantitative measurement of oxygen concentration and temperature have been developed and refined. In addition, the method is applied to measurement of flow velocity, based on the observed Doppler shifts of O_2 absorption lines. A prototype instrument incorporating these capabilities has been assembled and delivered to NASA Langley.

The technical approach used in this program combines two innovations or recent advances in an experimental system which results in a new capability for monitoring of oxygen and other major gas phase chemical species in high temperature flows. These innovations are: (1) the use of inexpensive GaAlAs diode lasers to measure gas phase species in high temperature flows; and (2) application of high frequency laser modulation and detection methods to obtain high sensitivity in absorption measurements using these lasers. The latter advance permits the development of a monitoring system with very wide dynamic range and fast time response. These innovations are particularly important in the detection of molecular oxygen since alternative detection methods are either intrusive (such as mass spectrometry or

electrochemical methods),[1] very expensive (non-linear laser methods such as CARS, or UV laser absorption/laser induced fluorescence,[2-3] both of which require very costly lasers), or insufficiently sensitive (UV absorption using lamps). While this effort is aimed at O_2 monitoring, similar approaches using diode lasers at other near-infrared wavelengths could be developed for detection of many other species in high temperature flows, such as H_2O, CO_2, CO, or fuel species.

The objectives of the Phase II research are outlined briefly in the following section. The basis of the experimental approach is described in detail in Section 3, and the results of measurements in laboratory flames are discussed in Section 4. Section 5 provides a description of the multi-channel fiber optic system designed specifically for the wind tunnel diagnostics. Section 6 provides a summary of the conclusions reached in this program as well as a discussion of other applications of the diagnostic and recommendations for further system improvements.

2. PHASE II RESEARCH OBJECTIVES

The primary objective of this Phase II research is to develop and demonstrate a prototype diagnostic instrument for nonintrusive measurement of O_2 concentration, temperature, and flow velocity in systems used in supersonic combustion research. The instrument utilizes fiber optics to direct the diode laser radiation into separate detection channels for simultaneous measurements along multiple lines of sight. The profiles of flow properties derived from such measurements can be used to determine important integrated performance parameters in scramjet propulsion testing, such as inlet mass capture and combustion efficiency.

The essential technical objectives of the Phase II program are:

(1) Development and testing of a fiber optic detection system for simultaneous measurements along multiple lines of sight.

(2) Laboratory calibration experiments to provide high accuracy for quantitative O_2 detection.

(3) Optimization of techniques for temperature measurement based on measured ratios of absorption by different O_2 lines.

(4) Adaptation of the absorption measurement technique for determination of flow velocity from observed Doppler shifts in the absorption line positions.

(5) Testing of a prototype instrument at the NASA Langley Research Center for measurement of O_2 concentration, temperature, and flow velocity.

3. DESCRIPTION OF MEASUREMENT APPROACH

3.1 Overview

This section provides an overall description of the measurement approach, including a discussion of the relevant molecular spectroscopy and a description of the operation of the near-IR diode lasers used for the diagnostic. The technique of high frequency wavelength modulation spectroscopy, which is used to achieve high sensitivity for measurement of small absorptions is then described. The technical approach for using the O_2 absorption measurements to determine O_2 concentration, gas temperature, and flow velocity is discussed. Finally, the laboratory measurement of critical spectral parameters (absorption line strengths) is described. The specific designs developed in this program for implementing the diagnostic for measurements in a flat flame burner and in wind tunnels are described in Sections 4 and 5, respectively.

3.2 Absorption Spectroscopy of Molecular Oxygen Using Near-IR Diode Lasers

3.2.1 O_2 Atmospheric Bands

The measurement technique is based on the absorption of monochromatic near-infrared laser radiation by molecular oxygen. Although vibrational bands of O_2 are infrared-inactive, electronic bands in the near-infrared spectral region can be used as the basis of an absorption diagnostic for measurement of O_2 concentrations. In particular, the $v' = 0 \leftarrow v'' = 0$ band of the magnetic dipole transition from the $X^3\Sigma^-_g$ ground electronic state to the excited $b^1\Sigma^+_g$ state occurs in a spectral region that is easily accessed by commercial GaAlAs diode lasers operating in the 760 to 780 nm range. The $b^1\Sigma \leftarrow X^3\Sigma$ band system of oxygen, which is known as the O_2 atmospheric band system, has been well characterized spectroscopically. Several quantitative studies of the $v' = 0 \leftarrow v'' = 0$ band (sometimes called the "A" band) have been performed,[4-6] yielding values for the line strength and line width parameters at room temperature. Line parameters for this band are tabulated in the HITRAN database prepared by the Air Force Phillips Laboratory/Geophysics Directorate,[7] and very precise values for line strengths, self-broadening, and air-broadening coefficients were obtained in the high resolution studies at room temperature by Ritter and Wilkerson.[6] More detailed results including some temperature-dependent data are available in the thesis by Ritter.[8]

The O_2 A band consists of P and R branches, each composed of pairs of lines designated PP and PQ (P branch) or RR and RQ (R branch).[9] These line pairs arise due to the splitting of the ground electronic state rotational levels (designated by rotational quantum number K″) into sublevels with total angular momentum J″ = K″, K″+1, and K″-1, with only odd values of K″ allowed. The upper electronic state has only singlet levels with J′ = K′, where only even values of K′ are allowed. The R branch spans a wavelength region from approximately 759.5 to 762 nm, while the P branch occurs at wavelengths longer than 762 nm. Commercially available diode lasers are better matched in wavelength to operation in the

R branch region. Laser operation in the R branch is advantageous for implementation of a temperature diagnostic, as described in Section 3.4. All measurements of O_2 in this program were made using lines in the R branch.

3.2.2 Near-IR Diode Lasers for High Resolution Spectroscopy

The diode lasers used in this program are standard commercial GaAlAs devices manufactured by Mitsubishi (Model ML4405) for applications such as compact disc players, bar code readers, and laser printers. Because these lasers are manufactured in very high volume, the unit cost is quite low (approximately $30 for small-quantity purchases). The ML4405 laser has a typical power of 3 mW, with a nominal wavelength (at room temperature) of 750 nm. Lasers with similar operating characteristics are available from other manufacturers (e.g., Sharp). The threshold current for these lasers is about 40 mA, with the 3 mW output typically achieved at about 50 mA operating current. At 50 mA and higher operating currents, the laser output spectrum is normally single mode; that is, the laser emission is confined to a single frequency with a line width of approximately 100 MHz. The laser wavelength may be coarsely tuned (tuning rate of approximately 0.25 nm $°C^{-1}$) by varying the laser case temperature over an operating range of -40 to +60 °C. Thus, by controlling the laser temperature, the wavelength may be tuned into coincidence with many O_2 absorption lines in the R branch region near 760 nm. We have tested and used numerous of these lasers during the course of this research. The laser distributor (ILX Lightwave) has been willing to pre-select lasers with room temperature wavelengths around 758 or 759 nm, so that only slight heating above room temperature (to temperatures of 25 to 30 °C) is required to tune the lasers into the O_2 absorption band.

High resolution tuning of the laser wavelength is accomplished by varying the laser diode injection current using an ILX Lightwave Model LDX-3620 battery powered low-noise current source. The instrumental width of the laser mode (~100 MHz, or 0.003 cm^{-1}) is small compared to the spectral width of the oxygen absorption lines (~0.04 cm^{-1} half width at half maximum for atmospheric pressure-broadened lines at room temperature or Doppler-broadened lines at 2000 K). This small spectral line width permits full resolution of the detailed molecular line shapes and also allows the selective measurement of an individual O_2 line without spectral interferences.

The laser as received is packaged in a hermetically-sealed window can (9 mm dia.). This package also contains a photodiode for laser power monitoring from the rear facet of the laser diode. For all of the experiments in this program, the laser package is housed in a commercial laser diode mount (ILX Lightwave Model LDM-4412) which is designed for precision-controlled thermoelectric cooling or heating of the laser (two TE coolers are contained in the mount). This mount is normally configured internally with a 0.5 NA single-element lens for collimation of the laser output beam. The approximate size of the mount is 2" (depth) × 4" (width) × 4" (height).

The laser temperature is regulated by a commercial controller supplied by ILX Lightwave (Model LDT-5910B). This unit monitors the resistance of a calibrated thermistor epoxied to the laser mounting plate and adjusts the current to the TE coolers to achieve a desired setpoint temperature. The temperature stability of this system is better than 0.01 °C.

The laser wavelength is calibrated using a Michelson interferometer wavelength meter (Burleigh Wavemeter). The wavelength meter readings, combined with comparisons of measured and tabulated O_2 spectra, are sufficient to permit unambiguous identification of the oxygen absorption lines. A confocal etalon (TecOptics SA300, free spectral range = 300 MHz) establishes a frequency scale for measurement of absorption line widths. A solid fused silica etalon (CVI Laser Corporation), with a free spectral range of 2.04 GHz (0.068 cm^{-1}) and a finesse of 30, is used to measure shifts in line position for determining flow velocity.

3.3 High Frequency Wavelength Modulation Spectroscopy

High frequency laser wavelength modulation spectroscopy (WMS) is used to measure the weak absorption signals observed in these experiments. We have described this technique in considerable detail in two recent publications, including comparisons with other high frequency diode laser detection methods (e.g. one- and two-tone frequency modulation spectroscopy).[10-11] Briefly, this method, which is an extension of diode laser "derivative spectroscopy" techniques widely used at kHz frequencies,[12] involves superposition of a small sinusoidal modulation on the diode laser injection current. Typically, the amplitude of the current modulation is chosen so that the induced wavelength modulation is comparable to the width of the spectral feature under study. Phase-sensitive electronics are then used to demodulate the detector photocurrent at the modulation frequency, f, or a harmonic, nf. By implementing this technique at sufficiently high frequencies, laser noise is minimal and detector-limited (ideally, shot noise-limited) sensitivity can be achieved. Our studies have shown that detection frequencies as low as 100 kHz are often sufficient to achieve these objectives, although the optimum frequencies are laser dependent. The distinction between WMS and FM spectroscopy (as described, for example, in Ref. 13) is mostly semantic – FM spectroscopy is defined as using modulation frequencies comparable to the absorption linewidths (~1 GHz or greater for the present experiment), whereas WMS uses modulation frequencies much smaller than the absorption linewidths. The distinction becomes important for high temperature measurements where Doppler broadened lines would require modulation frequencies well into the GHz regime using the FM schemes.

In the present work, we use 50 kHz modulation with second harmonic detection. The detector output is bandpass-filtered and amplified and sent to the RF input of a mixer (Minicircuits ZAD-8). The 50 kHz sine wave for laser current modulation is generated by a Wavetek Model 191 signal generator and fed to the external modulation input of the ILX laser current controller. The 50 kHz TTL reference output from the Wavetek signal generator is sent to a phase shifter/frequency doubler (Evans Electronics Model 4114)

and then used as the local oscillator input for $2f$ detection in the Minicircuits mixer. The mixer IF output is amplified and low pass-filtered before digitization.

The data acquisition system utilizes a 20 MHz 80386-based microcomputer (Northgate). This system uses a high speed 16-channel analog-to-digital converter board (Analog Devices RTI-860) that plugs into the microcomputer bus. The laser wavelength is repetitively scanned with an analog voltage ramp generated by a programmable waveform synthesizer (QuaTech WSB-10) which also plugs into the computer bus. Each A/D cycle is synchronized with the repetitive scanning of the laser wavelength for rapid averaging of the $2f$ signals. Typical parameters for a single scan are 512 data points, with a dwell time of 50 μs per data point. For most data taken in this study, 1000 such scans are co-added. Adaptation of this data acquisition system to multi-channel simultaneous detection is described in Section 5.

The second harmonic ($2f$) signals produced by WMS are directly proportional to absorbance, but the factor relating the $2f$ signals to absorbance at line center is best determined by direct experimental calibration. Ideally, such a calibration is done by comparing a direct transmission measurement of absorption with a $2f$ measurement for the specific absorption feature under study. In the present study, such calibrations are conveniently performed using suitable absorption path lengths in laboratory room air.

3.4 Spectroscopic Measurement of O_2 Concentration, Temperature, and Flow Velocity

3.4.1 O_2 Concentration

The measurement of O_2 concentration by diode laser absorption is based on straightforward implementation of Beer's law,

$$n = \alpha/\sigma\ell, \tag{3.1}$$

where α is the measured absorbance, σ is the absorption cross section, and ℓ is the absorption path length. In this expression, n is the O_2 number density, with units of cm^{-3}. The cross section at line center, σ_0, is related to the temperature-dependent absorption line strength, S(T), by

$$\sigma_0 = S(T) \cdot \phi(\nu_0), \tag{3.2}$$

where $\phi(\nu_0)$ is the line shape function. In the Doppler-broadened limit, which is a good approximation for measurements of O_2 at combustion temperatures and pressures of 1 atmosphere or less, $\phi(\nu_0)$ has a value of 0.47 $\Delta\nu_D^{-1}$, where $\Delta\nu_D$ is the Doppler half width at half maximum. In the pressure-broadened limit, $\phi(\nu_0) = (\pi\Delta\nu_L)^{-1}$, where $\Delta\nu_L$ is the pressure broadened (Lorentzian) half width. This limit is a good approximation for O_2 measurements at room temperature and atmospheric pressure. At intermediate temperature and pressure combinations, the line shape is described by a Voigt profile, which has the analytic form at line center of $\phi(\nu_0) = \phi_D \cdot \exp(a^2) \cdot \mathrm{erfc}(a)$, where ϕ_D is the Doppler line shape at line center, given above, and $a = \sqrt{ln2}\ (\Delta\nu_L / \Delta\nu_D)$.

From the above discussion, one can see that the determination of O_2 number density by the diode laser absorption technique depends on spectroscopic parameters that are functions of temperature. The temperature dependence of the line strength S(T) can be readily calculated to very high accuracy, as noted below. Thus, this parameter is well known at all temperatures provided that it has been accurately measured at one temperature. As described in Section 3.5, we conducted accurate laboratory measurements of the relevant O_2 line strengths at room temperature.

Two points should be noted concerning the temperature dependences contained in Eqs. 3.1 and 3.2. First, since the cross section is temperature dependent, best accuracy in measurement of number density requires knowledge of the gas temperature. In the present case, since gas temperature is itself a measurement objective, this information can be obtained by the techniques described below. In the more general case, where gas temperature may not be well characterized, uncertainties associated with imperfect knowledge of temperature can be minimized by selecting an absorption line with a cross section that is relatively insensitive to temperature over the range of temperatures expected. This point is discussed further in Section 4.4.

The second important point regarding temperature dependences is that temperature inhomogeneities along the line of sight may affect the accuracy of concentration measurements. The results of our flat flame burner studies, presented in Section 4, contain an example of how the accuracy of O_2 mole fraction measurements is degraded by a nonuniform temperature distribution across the line of sight. Again, these effects can be minimized by the careful selection of O_2 absorption line(s), as described in Section 4.4.

3.4.2 Temperature

Flow temperatures are determined by measuring the ratio of absorption signals for two O_2 absorption lines. This ratio is proportional to the ratio of line strengths, which depends only on temperature and known molecular parameters. The line strength ratio for two O_2 absorption lines is

$$\frac{S_1}{S_2} = \frac{S_1(T_0)}{S_2(T_0)} \exp\left[\frac{-hc\Delta E_{rot}}{k}\left(\frac{1}{T}-\frac{1}{T_0}\right)\right] \qquad (3.3)$$

where T_0 is a reference temperature (room temperature, for example) and ΔE_{rot} is the difference in lower state rotational energy for the two O_2 absorption lines. In the present study, we have mostly used a line pair consisting of the RQ(23,24) and RQ(33,34) lines, with lower state rotational energies of 791.034 cm^{-1} and 1605.806 cm^{-1}, respectively.[7] Figure 3.1 shows the ratio of the strengths of these two lines as a function of temperature. The sensitivity of temperature measurements using this line pair is best at temperatures below 2000 K, where the line strength ratio changes more rapidly with temperature.

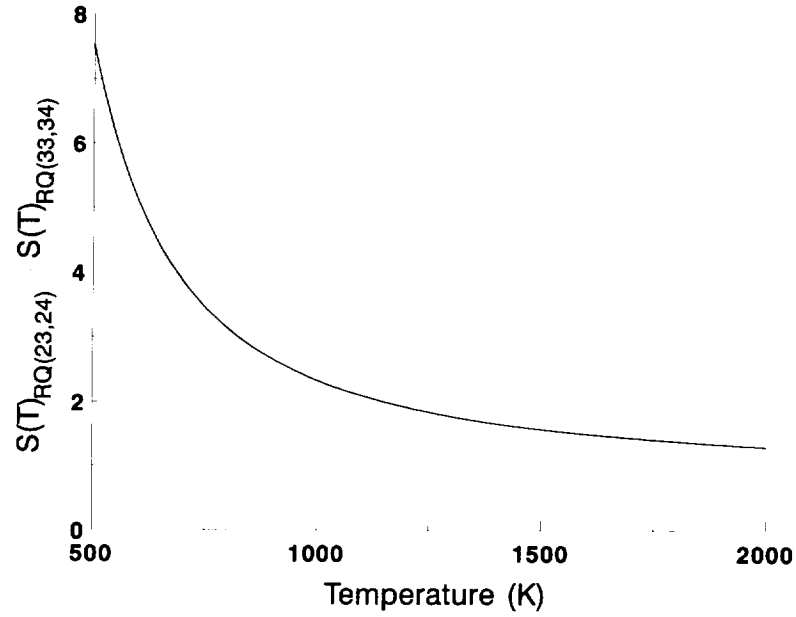

Figure 3.1. Temperature dependence of the line strength ratio for the O_2 line pair used in temperature measurements.

3.4.3 Flow Velocity

Measurement of flow velocity is perhaps the simplest of the three measurement objectives in this program. Velocity is determined by measuring the Doppler shift of the O_2 absorption line positions for lines of sight that have a directional component along the flow axis. Various strategies can be adopted for choosing the line of sight direction(s). An example is shown in Fig. 3.1. In this case two lines of sight are chosen through the flow, at angles θ and $-\theta$ measured with respect to a direction normal to the flow. The line center of the absorption peak is separated by a frequency difference

$$\Delta\nu = \nu_0 \cdot 2 \sin\theta \cdot v/c, \tag{3.4}$$

where v is the directed flow velocity and c is the speed of light. An advantage of using two lines of sight through the flow, rather than a reference line of sight through static gas, is that compensation for any pressure-induced shifts in line position is automatic. An etalon is used to establish the frequency scale in the spectral scans, as described in Section 3.2.2.

3.5 Laboratory Measurement of O_2 Spectral Parameters

To permit quantitative measurement of O_2 concentrations with minimum uncertainty, we sought absorption lines with maximum line strengths under the high temperature conditions of interest. In order for the absorption lines to be useful for measuring temperature simultaneously, however, the *ratio* of strengths for a chosen line pair must exhibit good sensitivity to changes in temperature. Furthermore,

these lines must be sufficiently separated from one another so that they are free of interferences, yet they must still be contained within the tuning range of a diode laser mode (typically ~1 cm^{-1}). Requirements for absorption lines to be used in velocity measurements are also covered by these constraints. Further discussion of other considerations in selecting O_2 absorption lines, depending on the measurement objective, is provided in Section 4.4.

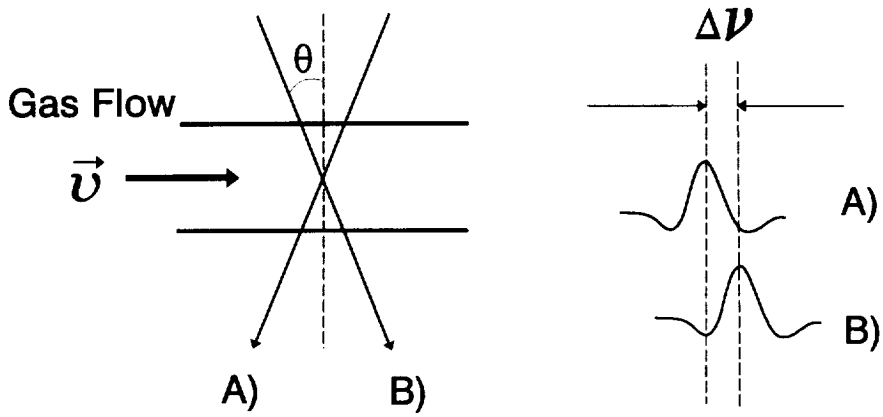

Figure 3.2. Determination of flow velocity by measurement of the separation of the Doppler shifted line center frequencies for two lines of sight.

As noted above, we chose the RQ(33,34) and RQ(23,24) absorption lines for the measurements of O_2 concentration, temperature and flow velocity. Figure 3.3 shows an experimental absorption spectrum of the RQ(33,34) and RQ(23,24) lines which was obtained with the wavelength modulation technique (50 kHz laser modulation, second harmonic detection). With line centers of the two absorption lines separated by 0.41 cm^{-1}, these features are well separated, yet they are contained within the typical tuning range of a single laser mode. The R-branch region of the O_2 absorption band is particularly convenient for temperature measurements, because absorption lines originating from rotational levels with significantly different energies occur at closely spaced frequencies.

We undertook careful measurements of the line strengths of the chosen lines under room temperature conditions in order to assess the reliability of previously reported cross sections and provide experimentally determined reference values for calculating line strengths at higher temperature. Accurate knowledge of the absorption line strengths provides the basis for quantitative measurement of O_2 number density and temperature using the diode laser instrumentation.

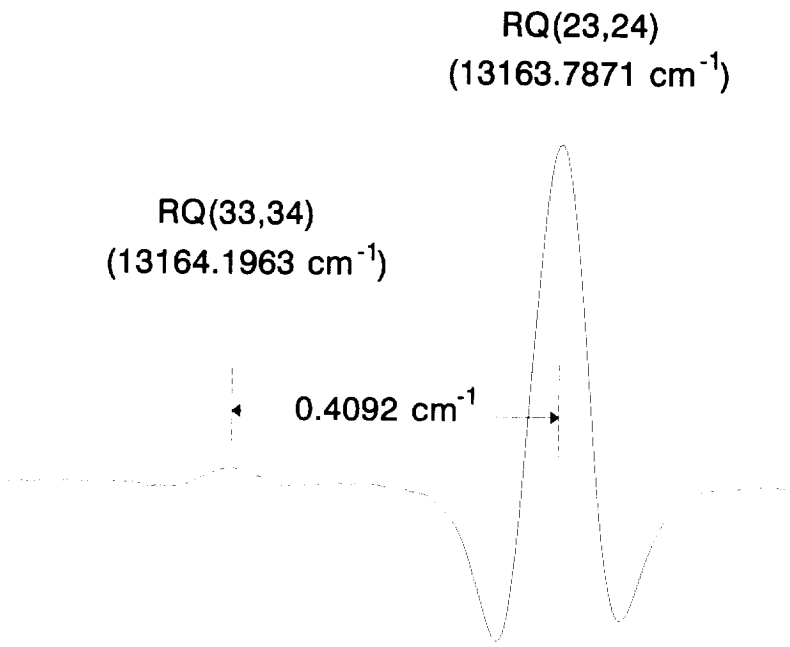

Figure 3.3. Experimental absorption spectrum showing the two O_2 lines selected for concentration, temperature, and velocity measurements.

For the line strength measurements, the diode laser output was divided by a 50/50 beamsplitter. One beam was sent to the confocal etalon for calibration of changes in the laser wavelength as the laser current is scanned. An optical isolator (Isowave I-80-UHP-A), installed between the etalon and the laser diode, eliminated optical feedback and enabled stable laser operation. The other beam was directed to a multipass O_2 cell (Herriott type;[14] 45 cm long, 30 passes), and the attenuation of the output intensity was monitored by a silicon photodiode (Centronic BPX-65). The signal from the photodiode was filtered and amplified (Stanford Research SR560), digitized with a transient digitizer (CAMAC Module DSP 2012S), and then stored in a microcomputer for later analysis.

To record the absorption spectrum of the RQ(23,24) and RQ(33,34) lines, we used a rapid scan method in which a train of saw tooth voltage ramps was applied to the laser current controller, resulting in repetitive wavelength sweeps across the region of interest. At a scan repetition rate of 100 Hz, averaging 1000 to 4000 sweeps resulted in direct absorption spectra with excellent signal to noise ratio for the RQ(23,24) line. As the O_2 pressure was varied from 600 Torr to 5 Torr, the peak absorbance of the RQ(23,24) line changed from 18% to 0.4% at 298 K. The peak absorbance of the RQ(33,34) line was about 30 to 35 times lower than the RQ(23,24) peak absorbance at each pressure, rendering accurate analysis of the weaker line difficult from direct absorption spectra. To improve the sensitivity of the RQ(33,34) line strength measurement, we used wavelength modulation spectroscopy (50 kHz laser modulation, second harmonic detection).

Direct absorption spectra of the RQ(23,24) line, obtained under several O_2 pressures, were fitted to Voigt profiles. From the fitted absorption line shape, the integrated absorbance was obtained at each O_2 pressure. Background absorbance, due to air in the laser beam path external to the absorption cell, was measured by evacuating the cell and was subtracted from each spectrum. Figure 3.4 shows the plot of integrated absorbance as a function of pressure as well as the fit obtained from a weighted linear least squares procedure. The strength of the RQ(23,24) line at 298 K, obtained from the slope of the fitted line, is $7.50 \pm 0.13 \times 10^{-25}$ cm^2 molecule^{-1} cm^{-1}. This result compares with the line strengths of $8.08 \pm 0.011 \times 10^{-25}$ measured by Ritter and Wilkerson[6] and 7.11×10^{-25} given in the HITRAN atmospheric line parameters compilation.[7] The original source of the HITRAN data is not specified, and no uncertainty estimates are available.

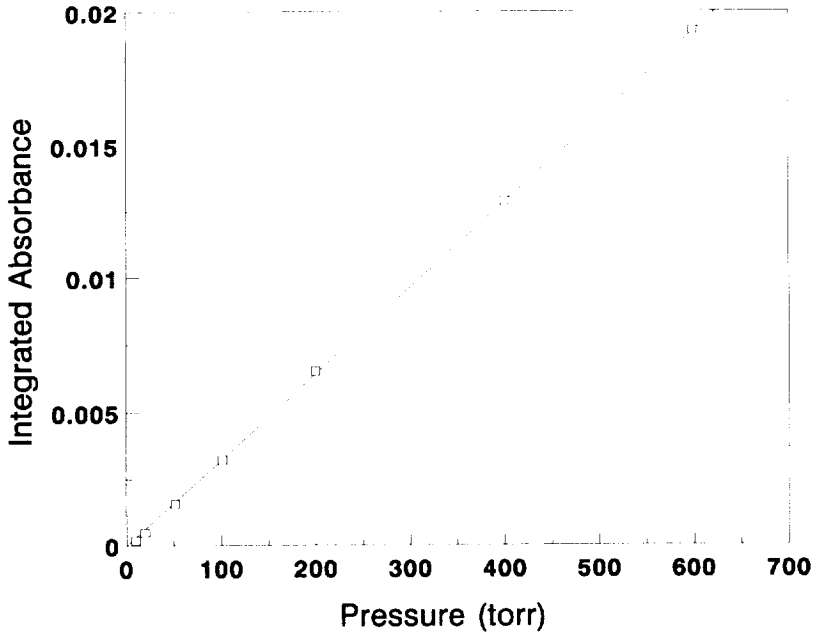

Figure 3.4. Measured integrated absorbance as a function of oxygen pressure for the RQ(23,24) absorption line.

There was a small characteristic mismatch in line shape between the calculated Voigt profile and the experimental absorption peak which could be attributed to collision-induced line narrowing.[6] Line shape expressions such as the Galatry profile can be used to account for this process that the Voigt profile ignores.[15] For the purpose of obtaining line strengths, however, we found the Voigt profile to be quite adequate since the area under the best-fit Voigt profile and the experimental peak agreed to within 2 to 3 percent over the full range of O_2 pressure which we employed. In measuring the pressure broadening coefficient, where the shape of the absorption peak and not the area determines the parameter, accounting for the line narrowing effect becomes more important.

For measurements of the weaker RQ(33,34) line using 50 kHz wavelength modulation, the wavelength modulation amplitude was optimized for biggest second harmonic ($2f$) signal at each O_2 pressure by actively monitoring the RQ(23,24) $2f$ signal on an oscilloscope while adjusting the current modulation amplitude. Second harmonic spectra were recorded using the rapid scan method. Averaging 1000 to 4000 sweeps resulted in $2f$ spectra with good signal to noise for data analysis. The background absorption spectrum from the room air path was recorded after each run with the Herriott cell evacuated. This background was subtracted from each experimental spectrum.

To determine the RQ(33,34) line strength from the $2f$ spectra, we measured the relative integrated $2f$ signal strengths of the RQ(23,24) and RQ(33,34) lines at each O_2 pressure. With the RQ(23,24) line strength already determined absolutely, we could then obtain the RQ(33,34) line strength from the measured ratio. In addition to the background subtraction, each $2f$ spectrum was normalized by the detected laser intensity to account for the variation of laser power with current. The difference in the pressure broadening coefficient for the RQ(23,24) and RQ(33,34) lines (0.0395 cm^{-1} atm^{-1} and 0.033 cm^{-1} atm^{-1}, respectively, from Ritter and Wilkerson[6]) was expected to affect the relative signal strengths of the $2f$ spectra. This effect was estimated by theoretical calculation, and a suitable correction was applied in the data analysis. The wavelength modulation theory used in these calculations is discussed in detail in Ref. 10. Weighted averaging of the measured signal strength ratios resulted in a ratio of the RQ(23,24) to RQ(33,34) line strengths of 37.90 ± 0.16. From this ratio, an RQ(33,34) line strength at 298 K of $1.98 \pm 0.04 \times 10^{-26}$ cm^2 $molecule^{-1}$ cm^{-1} is obtained.

The HITRAN compilation reports the RQ(33,34) line strength as 1.911×10^{-26}, corresponding to a line strength ratio of 37.19. Ritter and Wilkerson do not report a measurement of the RQ(33,34) line strength, but they describe several theoretical expressions that are available for calculating the relative O_2 line strengths. The theory that yields the best agreement with the Ritter and Wilkerson relative experimental line strengths is due to Watson. Using the Watson expression, we calculate the expected RQ(23,24)/RQ(33,34) line strength ratio at 298 K as 36.24. These comparisons indicate good agreement between our measured line strengths with currently available experimental and theoretical values.

4. LABORATORY FLAME MEASUREMENTS

4.1 Introduction

Measurements of O_2 concentration and temperature in premixed flames were performed using fuel-lean CH_4/O_2 mixtures in a laboratory flat flame burner. A single channel fiber optic system was used for these experiments. The motivations for the flame measurements were 1) to test the techniques for measurement of O_2 concentration and temperature, and 2) to assess the detection sensitivity of the fiber optic GaAlAs diode laser spectrometer under high temperature atmospheric pressure conditions. In this section, we describe the experimental details of the laboratory flame measurements, followed by presentation and discussion of the results.

4.2 Experimental Description

A block diagram of the experimental arrangement is shown in Fig. 4.1. For the premixed flat flame source, we used a burner from McKenna Products. The burner has a 6 cm diameter central core for the flame surrounded by an 11 mm annular shroud region for an inert gas flow to isolate the flame from room air. The CH_4 and O_2 gas flows are separately metered using Matheson variable area flow meters and then mixed prior to introduction into the flame region of the burner. The flow rate of the argon shroud gas is also metered using a Matheson flow meter. We limited our flame measurements to CH_4/O_2 equivalence ratios (Φ) of 0.4 and 0.6 because of very low O_2 absorbance levels at higher equivalence ratios. Fuel-rich flame conditions (Φ = 1.1) are also sometimes used to check or to correct for background signals when all of the flame O_2 is consumed.

The burner is mounted on a vertical translation stage with a micrometer adjustment, allowing us to probe 4 different heights (3, 5, 7, and 10 mm) above the burner surface. Since the flame is at atmospheric pressure (about 600 Torr for our laboratory in Santa Fe, New Mexico), we are confident that we are probing the post burn region. The gas flow rates for the premixed flames and the Ar shroud, and the O_2 mole fraction in the post burn region, are summarized in Table 4.1.

Table 4.1. The Gas Flow Rates and the O_2 Mole Fractions in the Flame.

Equivalence Ratio (Φ)	CH_4 (slm)	O_2 (slm)	Ar (slm)	O_2 Mole Fraction
0.4	0.85	4.25	2.13	0.50
0.6	1.18	3.92	2.13	0.31
1.1	1.83	3.27	2.13	0.00

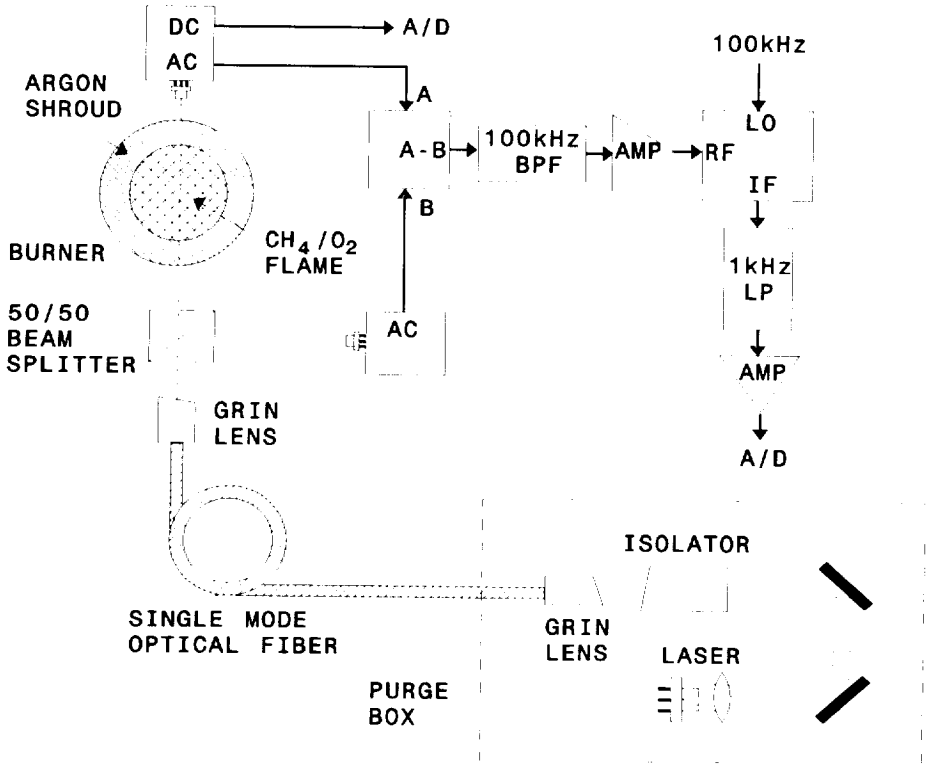

Figure 4.1. The experimental arrangement for measurements in the laboratory premixed flame using a single channel fiber optic diode laser system.

The laser output is gently focused with a three element lens assembly (Rodenstock 1403.108) and passed through the optical isolator (Isowave I-80-T(760); 2° angle polish on the input face) before impinging on the input fiber coupling GRIN lens. Two flat mirrors are used to extend the beam path length between the lens and the optical isolator, providing a small beam waist through the optical isolator and better matching of the input GRIN lens numerical aperture. The input GRIN lens is fused onto a single mode fiber and has a 6° angle polish on the front surface to minimize back reflection of the laser beam. Typically, about 15-20% of the diode laser output is coupled into the 4.7 μm single mode fiber core. The entire laser-to-fiber coupling system including the optical isolator is housed inside a purge box to remove the background oxygen in the optical path.

This design for coupling the laser output into the single mode fiber could be greatly simplified by using a fiber pigtailed laser with integral optical isolator. Such a system would also eliminate the need for a purge box. Unfortunately, such laser packaging in the 760 nm region is only available on a custom

basis. Our tests of two custom packages produced by two different vendors revealed unacceptable levels of background interference fringes.

For these laboratory measurements of temperature and concentration in the flame, we used a single channel fiber optic system. We tilted each optical surface at an angle along the laser beam path on the input side in order to minimize etalon fringes, but we still found residual etalon effects arising from the optical isolator surfaces and from the output fiber collimating GRIN lens surfaces. These etalon fringes, which were equivalent in amplitude to absorbances in the high 10^{-5} range, distorted the second harmonic absorption line shapes and baseline, rendering the data analysis difficult. Therefore, we chose to split the laser beam exiting from the single mode fiber with a 50/50 beam splitter so that we could subtract any background O_2 or etalon signals. One of the beams was used to probe the flame while the other (reference) beam traversed a short path of laboratory air such that the ambient O_2 signal in the reference path matched the ambient O_2 signal in the probe beam path. This matching of background signals was verified by operating the flame under the $\Phi = 1.1$ condition.

The two laser beams, after traversing either the flame region or the reference path, impinged on matched Si P-I-N photodiode detector/preamplifier modules (Analog Modules Model 310-46). This detector/preamplifier module allowed us to monitor both the AC output, with a gain of up to 60 dB, for extracting the absorbance signal, and the DC output with a gain of 20 dB for monitoring the laser intensity. The AC output from the reference leg was subtracted from that of the probe leg by combining both signals in a 180° RF combiner/splitter (Mini-Circuits ZSCJ-2-2). The resulting signal was then band-pass filtered at the 100 kHz second harmonic detection frequency and then fed to the RF port of a double balanced RF mixer (Mini-Circuits ZAD-8).

The 50 kHz TTL output from a Wavetek (Model 20) function generator, which generated the 50 kHz sine wave that was used to modulate the laser wavelength, was sent to a phase shifter/frequency doubler (Evans Electronics Models 4110, 4111) and the resulting 100 kHz reference signal was fed to the LO port of the RF mixer. The low frequency signal output from the IF port of the RF mixer was low-pass filtered (1 kHz) and amplified (60 dB) with a battery operated low noise filter/amplifier (SRS 560). The conditioned signal was then sent to an A/D port of the data acquisition system for storage and later analysis. The modulation amplitude of the 50 kHz sine wave was set while measuring O_2 at room temperature and atmospheric pressure to yield the optimum peak-to-trough amplitude in the resulting $2f$ signals; this modulation amplitude was maintained throughout the flame experiments.

The DC output from the detector/preamplifier was low-pass filtered and amplified and then fed to an A/D port for laser power monitoring. The second harmonic absorption spectrum was later normalized by the DC signal to account for variation in laser power as the laser current is scanned.

The data acquisition system consists of an 80386-based microcomputer (Northgate), fast multi-channel A/D converter board (Analog Devices Model RTI-860), and custom-developed software to acquire and store the data. The computer also controls a waveform synthesizer board (QuaTech Model WSB-10)

to generate a train of sawtooth shaped laser current ramps. The current ramp and the data acquisition cycle are synchronized by the computer software. Typically, the absorption signals from 100 or more current scans are coadded to improve the signal-to-noise of the acquired spectrum. For the flame measurements, we coadded 1000 current scans with each scan consisting of 512 data points with a dwell time per data point of 50 μs. The effective detection time constant is 50 ms (20 Hz detection bandwidth).

The flame temperature was measured at each equivalence ratio and vertical height with a Pt-Pt/13%Rh thermocouple (.015" bead diameter) by scanning the thermocouple across the flame and sampling the temperature at 2 mm radial intervals from the center of the flame through the Ar shroud to the ambient air. The thermocouple readings were corrected for radiation loss, as described in the results section below.

The flame measurements consisted of taking three runs of O_2 absorption spectra in fuel-lean flames at a given height and equivalence ratio, followed by a fuel-rich (Φ=1.1) flame run to take the background absorption spectrum. The equivalence ratio or the vertical height of the fuel-lean flame was then changed and the procedure was repeated. The transmitted laser power as a function of laser current was recorded at regular intervals from the DC output of the photodiode detector/preamplifier. After all the flame measurements were made, two room temperature O_2 absorption spectra were taken for use in absorbance calibrations, as described below. Finally, the flame temperature at a given height and equivalence ratio was measured using the thermocouple.

4.3 Experimental Results

4.3.1 Flame Temperatures

The second harmonic absorption spectra of O_2 in fuel-lean flames were first processed by subtracting fuel-rich (Φ = 1.1) background runs to remove etalon effects and then corrected for the laser power variation (I_0) across the spectrum by dividing by the DC output spectra. Figure 4.2 shows the O_2 second harmonic absorption spectra from the flame measurements after these corrections were applied.

The ratio of intensities of the RQ(23,24) and RQ(33,34) lines, determined from the peak-to-trough amplitudes of the $2f$ line shapes, was assumed equivalent to the line strength ratio, and the effective flame temperatures were obtained from the known dependence of the line strength ratio on temperature. These flame temperatures are indicated by the filled circles in Figure 4.3(a) and (b) for the Φ = 0.4 and 0.6 flame, respectively. Shown for comparison are the averages of the thermocouple readings at each flame height.

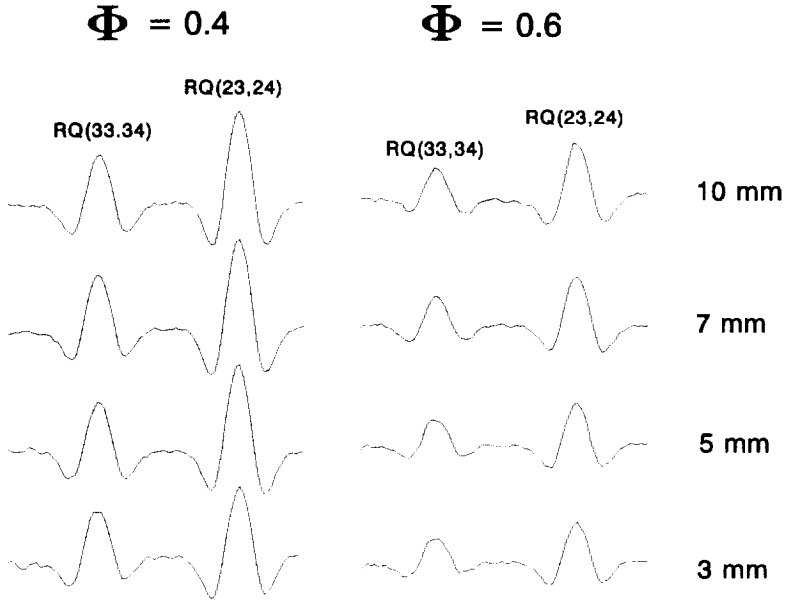

Figure 4.2. Normalized second harmonic absorption spectra of the O_2 RQ(23,24) and RQ(33,34) line pair for the Φ = 0.4 and 0.6 flame conditions.

The thermocouple measurements of the flame temperature profiles were corrected for radiation loss by[1]

$$\Delta T = \frac{(\sigma \varepsilon d)}{(N_u k)} (T_{tc}^4 - T_b^4), \qquad \textbf{(4.1)}$$

where N_u (Nusselt Number) = 2 + 0.236 $Re^{0.606}$ $Pr^{1/3}$, Re (Reynolds Number) = (ρ v_{gas} d)/μ, Pr (Prandtl Number) = (μ c_p)/k, σ = Stefan-Boltzmann constant, ε = thermocouple emissivity, d = thermocouple bead diameter, T_{tc} = thermocouple temperature, T_b = background temperature, ρ = gas density, v_{gas} = gas flow velocity, μ = gas viscosity, c_p = specific heat, and k = thermal conductivity. The Nusselt number was taken from Ref. 17, while the emissivity for a Pt-Pt/13%Rh thermocouple was taken from Ref. 18. The uncorrected and corrected thermocouple measurements for the Φ = 0.4 flame at two vertical positions are shown in Figure 4.4. The magnitude of the radiation correction in the "flat" portion of the flame is about 180 K. We also observe that the temperature boundary layer expands as the flame propagates upward, and the "flat" portion of the temperature drops about 100 K between flame heights of 3 mm and 10 mm.

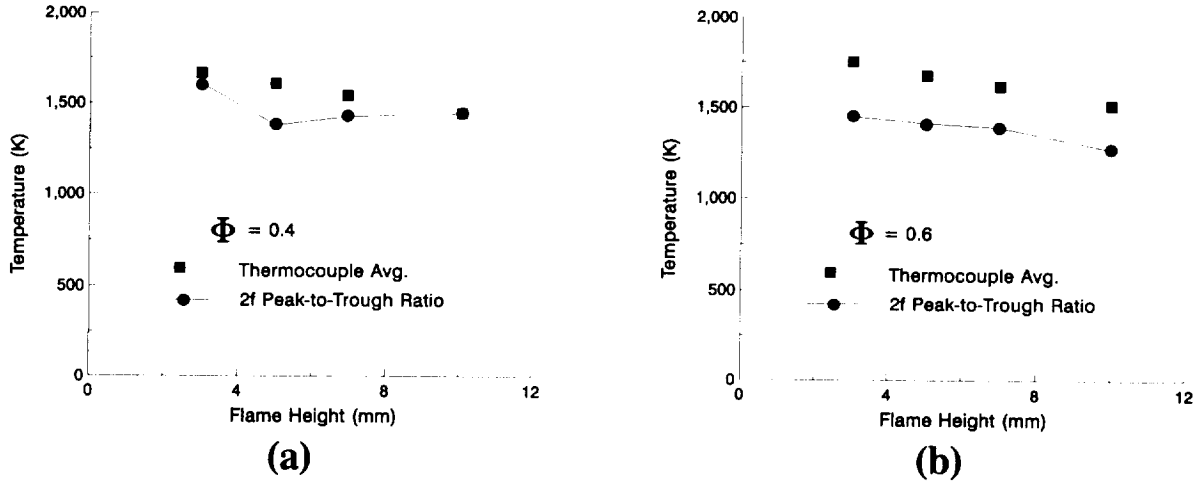

Figure 4.3. Effective flame temperatures inferred from the intensity ratio of the RQ(23,24) and RQ(33,34) lines, and the average temperatures measured using a thermocouple.

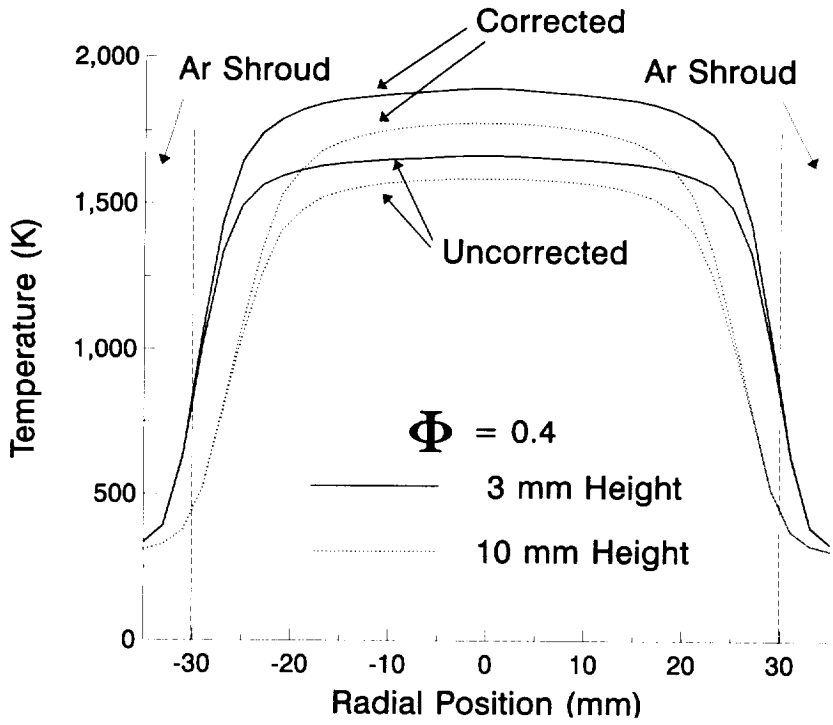

Figure 4.4. Radial profiles of the flame temperature (Φ = 0.4), showing uncorrected and corrected thermocouple measurements.

The average thermocouple measurements plotted in Fig. 4.3 are simple unweighted arithmetic means of these profiles. While the flame temperatures inferred from the O_2 absorption spectra follow the averaged thermocouple measurements at least qualitatively, we wish to examine the cause of the discrepancies in greater detail. In deriving the spectroscopic flame temperatures, we have assumed that the $2f$ peak-to-trough ratios are equivalent to the line strength ratios, without considering differences in line broadening. Furthermore, the thermocouple measurements should be weighted by the variation of O_2 density and peak cross sections across the flame in making comparisons with the spectroscopic measurements. We will consider these issues in detail in Section 4.4.

4.3.2 O_2 Concentrations

The peak-to-trough amplitude of the $2f$ signal varies linearly with absorbance, but the calibration factor relating the $2f$ signal to absorbance is best determined experimentally. In these measurements, we used the room temperature O_2 absorption spectra obtained in laboratory air for the absorbance calibration. Transferring this calibration to the measurements taken under flame conditions requires proper accounting for differences in the absorption line shapes between room temperature and flame temperatures. In particular, the room temperature absorption lines used for calibration are predominantly pressure broadened, whereas Doppler broadening dominates in the flame spectra.

We use the theoretical treatment of wavelength modulation spectroscopy presented by Silver[10] of our laboratory to calculate the appropriate corrections to the absorbance calibration measured at room temperature. The second harmonic signal amplitude, for a fixed absorbance and a given line shape, depends on the ratio of the wavelength modulation amplitude to the absorption line width (the modulation index). At the modulation index producing the maximum room temperature second harmonic signal, the calculated $2f$ signal amplitudes (peak-to-trough) relative to unit absorbance are 0.57 for the room temperature line and 0.65 for the same O_2 line at the spectroscopically determined temperature for the $\Phi = 0.4$ flame at 3 mm. These and similarly calculated peak heights for the other flame conditions are used as correction factors in transferring the room temperature calibration to flame conditions.

Having determined the experimental O_2 absorbances (α) in the flame using this procedure, the experimental O_2 number densities may be calculated from Beer's law, Eq. 3.1, where the absorption path length is $\ell = 6$ cm. The line center absorption cross section (σ_0) for each flame height and stoichiometry is calculated from the line strength ratio S(T) and the Voigt line shape for the flame pressure and temperature. In these calculations, we use the spectroscopic effective flame temperatures, determined in the manner described above, and we assume that pressure broadening coefficients scale as $T^{-0.76}$.[8] The analysis is insensitive to this latter assumption, since Doppler broadening is dominant under our flame conditions. Finally, experimental O_2 mole fractions are obtained by dividing the O_2 number densities from Eq. 3.1 by the total gas number density in the flame (again using the spectroscopic effective flame

temperature). These experimental mole fractions, obtained separately from the measured RQ(23,24) and RQ(33,34) absorbances, are shown in Fig. 4.5.

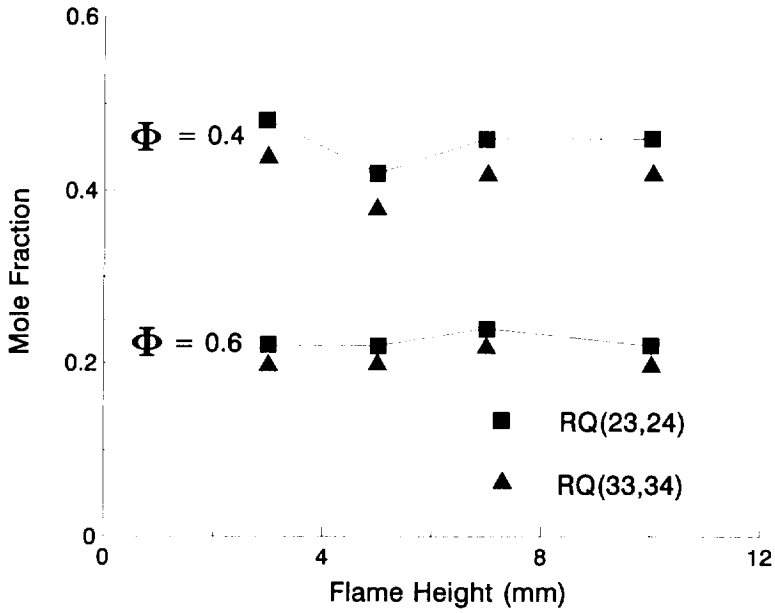

Figure 4.5. Experimental O_2 mole fractions obtained from RQ(23,24) and RQ(33,34) $2f$ absorption features and the experimental effective flame temperatures.

The average experimental O_2 mole fractions from the Φ = 0.4 and 0.6 flames are 0.44 and 0.22, respectively, while flame stoichiometry predicts 0.50 and 0.31. Differences between the experimental mole fractions and the predicted values are examined below.

4.4 Discussion

4.4.1 Flame Temperatures

As shown in Figure 4.4, there are strong temperature gradients near the flame/Ar shroud boundary. These temperature gradients give rise to variation in the O_2 number density (although mole fraction is constant) and absorption line strength along the line-of-sight path across the flame. In order to better understand the influence of these temperature gradients on our spectroscopic measurements of temperature and mole fraction, we calculated the expected direct absorption spectrum and the corresponding second harmonic spectrum for the RQ(23,24) and RQ(33,34) lines using the measured (thermocouple) temperature profiles and the assumption of uniform O_2 mole fraction determined by flame stoichiometry.

For these calculations, the absorption line of sight is represented by thirty segments of equal length (2 mm), each characterized by a local temperature obtained from the radiation-corrected thermocouple measurements. For each segment, the absorption line strengths and line shapes for both O_2 lines are

calculated from the known temperature, and the O_2 number density is calculated from the known mole fraction and total gas number density. The O_2 line center absorbances within the segment are then determined from Eq. 3.1. The absorption line profiles across the full line of sight are obtained by summing the contributions of the thirty segments. The corresponding second harmonic spectra are calculated using the theory described by Silver.[10] Since the O_2 absorption line width varies across the flame, an effective modulation index, which is the average of the modulation indices for the thirty segments, is used in this latter calculation. This calculation procedure was performed for the conditions corresponding to each of the laser absorption experiments.

The ratios of the calculated second harmonic peak-to-trough intensities were compared with the calculated direct absorption area ratios for the RQ(23,24) and RQ(33,34) lines. The direct absorption area ratio is, by definition, equal to the ratio of line strengths. The ratio of $2f$ intensities may be somewhat different, however, due to differences in pressure broadening of the two lines. We used these calculated ratios to correct the experimental $2f$ ratios in order to obtain a more accurate representation of the experimental ratios of line strengths. These corrected experimental ratios were then used to derive a new set of flame temperatures, plotted in Fig. 4.6. The effect of this correction is to slightly lower the experimental temperature values. Also shown in the figure are the temperatures derived from the ratios of absorption line areas obtained from our detailed piecewise calculations. Figure 4.6 should be viewed as providing a comparison between our experimental temperature results and the "exact" line-of-sight averaged temperatures, based on our knowledge of flame stoichiometry and temperature profiles.

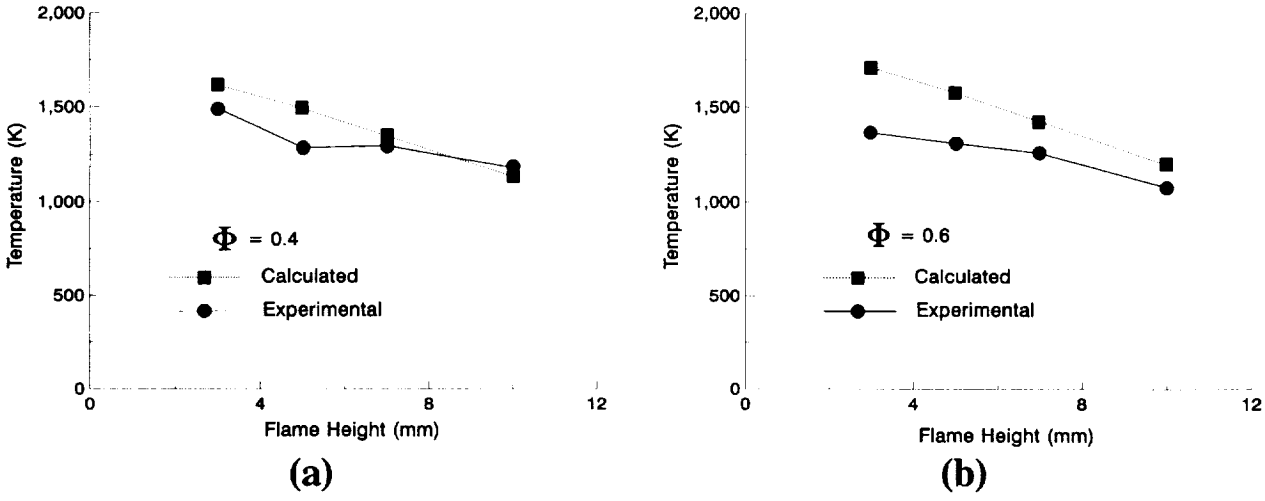

Figure 4.6. Comparison of the experimental flame temperatures with the exact line-of-sight averaged temperatures (designated as "calculated" temperatures).

The radiation-corrected thermocouple measurements, which are used in our exact calculation procedure described above, are subject to errors arising from catalytic reactions between the Pt/Pt-13% Rh thermocouple and the flame, and surface contamination of the thermocouple at high temperature by elements such as hydrogen and carbon. Some researchers have addressed these issues by applying different types of protective coatings on the thermocouple bead.[19] We believe that fuel-lean CH_4/O_2 premixed flames in the post burn region are not highly susceptible to these complications since methane, carbon, or hydrogen should have completely reacted and formed stable combustion products (H_2O and CO_2) in the post burn region, and the catalytic effects seem most severe in hydrogen-rich, low pressure flames with stretched reaction zones.[19] Therefore, we estimate the uncertainty in the corrected thermocouple temperatures to be about 10%, which is the approximate magnitude of the radiation correction.

The experimental flame temperatures show the same qualitative trend as the calculated exact temperatures in that the apparent temperature decreases as higher portions of the flame are probed. The quantitative agreement between the experimental and exact temperatures for the $\Phi = 0.4$ flame seems satisfactory, but the experimental temperatures are systematically low for the $\Phi = 0.6$ flame. In fact, the experimental temperatures for the $\Phi = 0.6$ flame are actually lower than for the $\Phi = 0.4$ flame, even though the thermocouple data indicate the expected result that the flame temperatures are higher. We attribute the poorer agreement of the $\Phi = 0.6$ temperature data to the reduced O_2 signal levels as compared to the leaner flame. In particular, the magnitudes of the O_2 signals and the background etalon fringes in the $\Phi = 0.6$ data are comparable, so that possible systematic errors in our background subtraction procedure may be more significant.

4.4.2 O_2 Mole Fractions

As noted in Section 4.3, the O_2 mole fractions derived from the spectroscopic data are lower than the mole fractions calculated from flame stoichiometry. In this discussion, we examine the reasons for this discrepancy by again referring to our "exact" calculations of O_2 absorbance along the flame lines of sight. By comparing our measured absorbances with the calculated values, we find agreement to within about 4% (averaged over the two O_2 lines and the four heights that were probed) for the $\Phi = 0.4$ flame and to within about 15% for the $\Phi = 0.6$ flame. Thus, the agreement between the measured and expected values of absorbance for the given flame conditions is actually quite good, and the low experimentally derived values for mole fraction cannot be attributed to poor accuracy in our measurements of O_2 absorption.

We can analyze our exact calculations of line-of-sight absorbance and effective flame temperature to derive "calculated" mole fractions, in a manner identical to our analysis of the spectroscopic data. Figure 4.7 shows a comparison of the experimental and calculated mole fractions, and the mole fractions expected from flame stoichiometry are also shown. In this case the "experimental" values for mole

fraction that are plotted are determined using the revised experimental temperatures that are shown in Fig. 4.6. Only the experimental results obtained from measurements using the RQ(23,24) absorption line are plotted in Fig. 4.7. The disagreement between the calculated and experimental O_2 mole fractions is expected since we have noted some disagreement between the experimental and exact line-of-sight temperatures, and the experimental absorbances differ slightly from the calculated absorbances as discussed above. In fact, the values derived for mole fraction are quite sensitive to temperature, as can be seen by comparing the experimental values shown in Fig. 4.7 with the values presented earlier in Fig. 4.5, where somewhat higher flame temperatures were used in the analysis. The sensitivity of these measurements to uncertainties in temperature, or even to temperature variation along the line of sight, can be minimized by appropriate choice of O_2 absorption line, as described below.

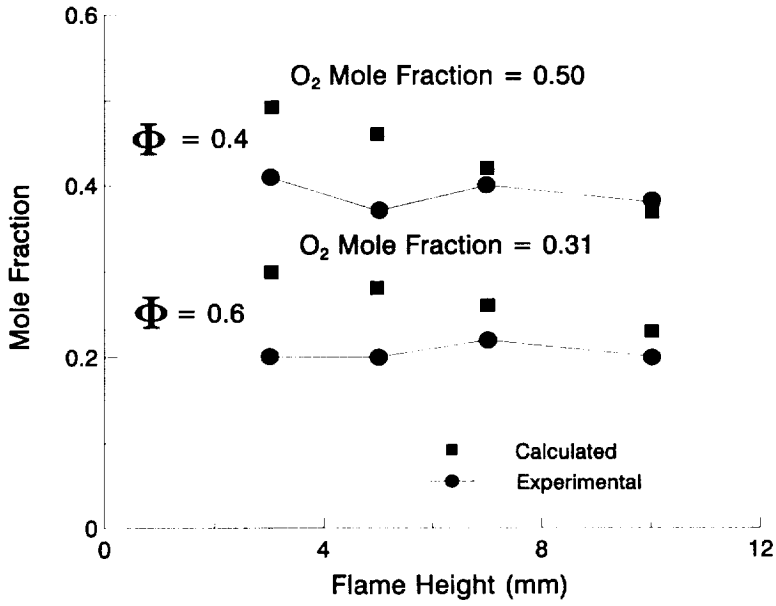

Figure 4.7 Experimental and calculated line-of-sight integrated O_2 mole fractions, and the expected O_2 mole fractions from the flame stoichiometry.

In order to assess the sensitivity of the mole fraction measurements to the temperature gradient, we can write Beer's law for the case of line shape dominated by Doppler broadening and uniform pressure across the line of sight as

$$\alpha = \sigma\, n\, \ell \cong \frac{S(T)}{1.06\,\Delta\nu_D}\,\frac{x_{o_2}\,p}{k\,T}\,\ell \propto \frac{S(T)}{T^{1.5}}\,x_{o_2}. \qquad \textbf{(4.2)}$$

Equation 4.2 shows that a single line of sight absorption measurement, under conditions where Doppler broadening predominates, weights the O_2 mole fraction by $S(T) \cdot T^{-1.5}$, where S(T) is the temperature-

dependent line strength. In the case where the O_2 mole fraction can be presumed uniform across the line of sight, as in the premixed flat flame, the best chance of retrieving an accurate mole fraction from a line of sight absorption measurement is achieved when the weighting function $S(T) \cdot T^{-1.5}$ has minimal variation across the line of sight. We can attempt to achieve this condition by choosing an absorption line with lower state rotational energy such that $d[S(T) \cdot T^{-1.5}]/dT \cong 0$ over the range of temperatures encountered across the line of sight. Carrying out this differentiation yields the result

$$E_{rot} = \frac{5kT}{2hc} + \frac{\nu e^{-hc\nu/kT}}{1 - e^{-hc\nu/kT}} \qquad \textbf{(4.3)}$$

where $\nu = 1556$ cm^{-1} is the O_2 vibrational frequency.

At T = 1500 K, which is typical of flame temperatures in our experiments, $E_{rot} = 3057$ cm^{-1} is obtained from Eq. 4.3. An O_2 absorption line with this approximate lower state rotational energy is the RR(45,45) line, with $E_{rot} = 2956$ cm^{-1}.

In Figs. 4.8 and 4.9, the weighting function $S(T) \cdot T^{-1.5}$ for the RQ(23,24) and RQ(33,34) lines, normalized by its value at the center of the flame, is plotted as a function of flame radial position. The weighting function is also plotted for the RR(45,45) rotational line. The flame temperature profiles measured with the thermocouple for the $\Phi = 0.4$ flame are used in constructing these plots.

The plots in Fig. 4.8, at a height of 3 mm above the burner surface, show that both the RQ(23,24) and RQ(33,34) lines weight the cooler edges of the flame more strongly than the uniform high temperature region. Further, the mean value of the normalized weighting function is greater than unity so, from Eq. 4.2, we expect that measurements on either line would underestimate the true O_2 mole fraction. In contrast, we see that the normalized weighting function for the RR(45,45) line is very close to unity over the entire optical path, dropping only at the very edge of the flame. Thus we expect that absorption measurements using the RR(45,45) line should yield accurate results for O_2 mole fraction at this height above the burner.

Figure 4.9, showing plots of the normalized weighting function for a height of 10 mm, indicates again that both the RQ(23,24) and RQ(33,34) lines are expected to yield inaccurate values for O_2 mole fraction. The figure shows that the RR(45,45) line again has a value of the normalized weighting function that is close to unity over a significantly broader region of the flame than either of the two lower energy lines. Also, the weighting function for this line becomes small near the cool edges of the flame, showing that the absorption line is really probing the hotter portion of the flame while ignoring most of the cooler edges. Thus, a reasonably accurate value for O_2 mole fraction might still be extracted in this case, particularly if an effective path length somewhat shorter than the full path across the flame is used in the data analysis. Figure 4.9 should be compared with Fig. 4.4 to understand the surprising extent to which the appropriate choice of absorption line can compensate for the effects of a nonuniform temperature profile.

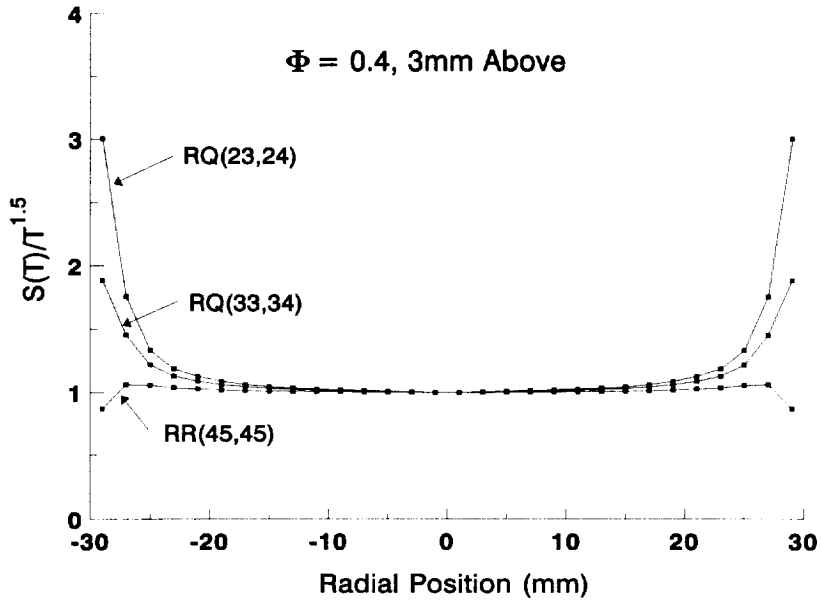

Figure 4.8. $S(T) / T^{1.5}$ vs radial position at 3 mm above the burner for the $\Phi = 0.4$ flame for the RQ(23,24), RQ(33,34), and RR(45,45) rotational lines.

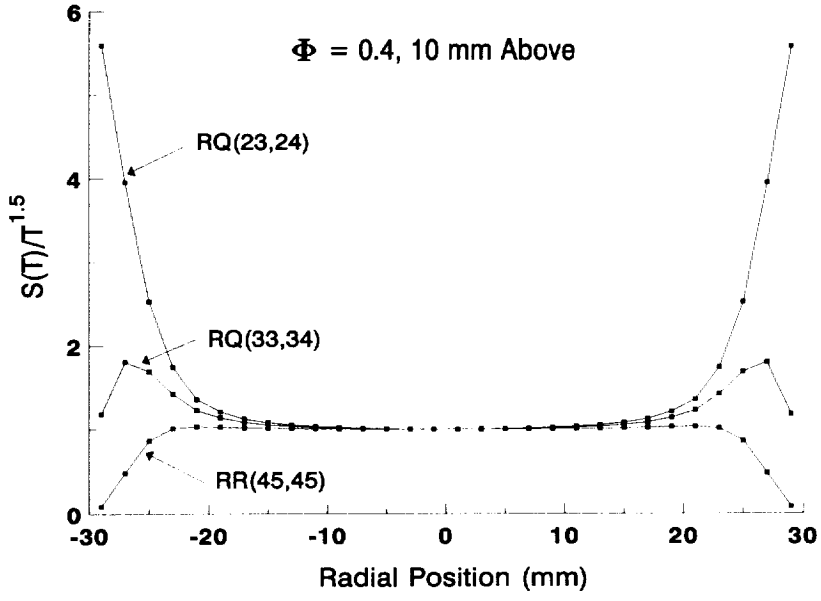

Figure 4.9. $S(T) / T^{1.5}$ vs radial position at 10 mm above the burner for the $\Phi = 0.4$ flame for the RQ(23,24), RQ(33,34), and RR(45,45) rotational lines.

Unfortunately, for the conditions that apply in our premixed flame experiments, the absorbance of the RR(45,45) line is expected to be about six times weaker than that of the RQ(33,34) line. Given the difficulties that we experienced with unwanted interference fringe effects, signal to noise is not adequate to permit the use of this line in the flame unless a multiple pass optical design is used. We find from Eq. 4.3 that the RQ(33,34) absorption line is expected to be well suited to O_2 mole fraction measurements for average temperatures around 700 K. Thus, at least for the conditions studied by the University of Virginia group,[20] we expect that the RQ(33,34) line should be suitable for O_2 mole fraction measurements in Langley wind tunnels.

4.4.3 2*f* Detection Sensitivity

Perhaps the most significant technical challenge that we faced during this Phase II effort was the occurrence of unwanted etalon effects arising from pairs of optical surfaces along the laser beam path. By minimizing the number of optical surfaces, we have previously achieved 3×10^{-7} minimum detectable absorbance in a 1 Hz bandwidth.[21] This detection sensitivity is by far the best that we have observed with near-IR GaAlAs laser diodes and was achieved in an optical path where no fiber optics were used.

The development of the fiber optic system used in this study resulted in the inclusion of several optical surfaces along the laser beam path, including an optical isolator (Faraday rotating crystal and polarizers), input and output collimating GRIN lenses, and the fiber splitter and connectors. These surfaces, when not properly tilted at an angle with respect to the laser beam axis, create unwanted etalon effects and greatly reduce the detection sensitivity. In the premixed flame measurements described in this section, subtraction of background interference fringes from the acquired spectra was necessary before we could start the data analysis.

Figure 4.2 shows 2*f* spectra of O_2 in fuel-lean flames at different heights above the burner. The weakest 2*f* absorption feature, the RQ(33,34) line in the $\Phi = 0.6$ flame at 3 mm height, corresponds to about 8.1×10^{-5} absorbance. With signal-to-noise of 20 to 1, we estimate the minimum detectable absorbance to be about 4×10^{-6}. A 1 kHz low pass filter was used at the final stage of signal conditioning, while the A/D conversion step utilized a dwell time of 50 μs per data point. Coadding 1000 scans results in a detection bandwidth of between 1 Hz and 20 Hz.

The level of background interference fringes as estimated from the fuel-rich flame runs appears to be about 4×10^{-5} in equivalent absorbance. The spacing of the fringes is similar to the separation of the two absorption features in our spectra. The separation of two surfaces responsible for creating such fringes is about 8 mm for an index of refraction of 1.5. We believe the source of this etalon to be the output collimating GRIN lens. Subtracting fringes of magnitude 4×10^{-5} from an absorbance spectrum where the absorbance signal is only about 8×10^{-5} (as was the case for the $\Phi = 0.6$ flame at 3 mm height) suggests the possibility of substantial systematic error being introduced in the data analysis. As we have

previously discussed, such systematic error may be the cause of larger discrepancies between the expected and experimentally derived flame temperatures and mole fractions in the $\Phi = 0.6$ flame.

4.5 Conclusion

The spectroscopic measurement of temperature and concentration of O_2 in premixed flat flames, using a fiber optic-coupled GaAlAs near-visible diode laser system was presented. The spectroscopically measured flame temperatures were compared against the temperatures derived from calculated data, which were based on the radiation corrected thermocouple measurements. These experimental and calculated temperatures were found to agree to within about 7% in the $\Phi = 0.4$ flame and about 15% in the $\Phi = 0.6$ flame. The spectroscopic determination of O_2 concentrations, expressed as mole fraction of O_2 in the flames, showed a 10 to 20% deviation from the expected mole fraction in the $\Phi = 0.4$ flame and about 30% deviation in the $\Phi = 0.6$ flame.

Our analysis based on the line-of-sight integrated spectral simulation using the thermocouple temperatures showed that good agreement between spectroscopically determined mole fractions and the values expected from flame stoichiometry should be possible at the 3 mm flame height but that the agreement degrades at higher positions above the burner. This result was traced to the temperature sensitivity of absorbance using the chosen absorption lines. Under the premixed flame conditions used in this study, the RR(45,45) line shows substantially less sensitivity to the nonuniform temperature fields encountered in the flame, but at a cost of a 6 times reduction in signal level compared to the RQ(33,34) line.

Finally, the sensitivity expressed as minimum detectable absorbance was found to be 4×10^{-6} at a detection bandwidth of 1 Hz or higher. This sensitivity was achieved only by subtraction of background interference fringes, however.

5. MULTI-CHANNEL FIBER OPTIC SYSTEM

5.1 Introduction

Previous sections of the report have presented the technical approach and have described in detail certain experimental configurations that were used in laboratory experiments at Southwest Sciences. In this section, we briefly describe the design features of the diagnostic that are particularly related to multi-channel measurements using a fiber optic system. A detailed step-by-step discussion of the operation of this system is contained in the Instrument Manual, included as an appendix to this report.

5.2 Optics and Electronics

The "front end" of the optical system is quite similar to that described for the flat flame burner measurements in Section 4 . The output from the Mitsubishi ML4405 diode laser is coupled into a single mode fiber in exactly the same manner previously described. In this case, however, a 30-meter length of single mode fiber is used after the input coupling GRIN lens. This fiber is directly fusion spliced onto the input of a 1 × 4 fiber splitter (Amphenol). A GRIN lens is fusion-spliced onto each of the four output fibers (each output fiber is about 2 meters in length). With this arrangement, the 1 × 4 splitter is located adjacent to the wind tunnel or other facility where diagnostic measurements are to be made, while the long run of fiber cable on the input side allows the laser, controlling electronics, and data acquisition system to be located in a separate control room.

The system described above results in output power levels of approximately 10 μW in each of the four channels when approximately 1.5 mW of laser power is available at the output of the isolator. We typically experience about 15 to 20% coupling efficiency into the single mode fiber, and the remaining losses are due to transmission losses over the long fiber run and losses in the splitter. After first experimenting with fiber connectors at various locations in the system, we elected to work with this fusion-spliced system in order to minimize losses. We had initially tested a 1 × 8 splitter, however, the available power in each output channel was too low. As higher power diode lasers become available in this wavelength region, increasing the number of channels to 8 or higher may become feasible.

For the detector side of the optical system, we elected to collect the transmitted light directly on large-area Si photodiodes. This design minimizes losses due to beam steering in the flow. Analog Modules Model 310-46 preamplifiers with AC and DC outputs are used to condition the detector outputs, as in the flat-flame burner experiments described previously. RF mixers (Mini-Circuits ZAD-8) are used to demodulate the AC signals at $2f$, and the demodulated $2f$ signals and DC signals are further amplified and low-pass filtered using Pacific Instruments Model 3100 signal conditioning amplifiers. The amplified and filtered $2f$ signals are normalized by the detector DC outputs using Analog Devices divider chips (Part No. AD 734). Finally, these normalized signals are sent to the fast A/D system described below for digitization, signal averaging, and storage. The normalization of the $2f$ signals by transmitted laser power

accounts for such effects as variation in the laser power as a function of wavelength, differences in laser power in the four channels, and changes in transmitted laser power due to beam steering effects or particulates in the flow. The $2f$ signals that are normalized in this fashion are directly proportional to absorbance.

5.3 Data Acquisition

The instrument includes a PC-based data collection system that can handle up to sixteen data input channels. Southwest Sciences has provided a program, OXY, to control the laser and to digitize and store the O_2 wavelength modulation spectra. Data collection is performed at nearly unit duty cycle and the maximum running time is limited only by the amount of system RAM; typical set-up conditions permit 3½ minutes of continuous measurement. The data collection hardware includes a 2048-point arbitrary waveform synthesizer (QuaTech WSB-10) and a 16-channel fast A/D converter with 12-bit resolution (Analog Devices RTI-860) that are used to sweep the laser wavelength and to digitize the demodulated signals, respectively. In addition, an inexpensive I/O board (Keithley-Metrabyte DAS-4) is included to detect a hardware trigger signalling the start of an experiment.

OXY uses a graphic menu display allowing the user to select the number of input channels (up to 16), the number of digitizations per sweep, the dwell time per digitization (minimum 5 μs), the number of sweeps to co-add per spectrum, and the fraction of each scan allocated as "dead time" for the laser and electronics to settle between saw-tooth sweeps. The user can also select the number of data arrays to be kept in memory which, in turn, varies the data collection duty cycle (see below). After leaving the set-up menu with a "RUN" command the user is prompted for a descriptive tag (up to 64 characters) for the experiment, then the program switches to idle mode which starts the laser-scanning ramp, performs digitizations and displays averaged scans of all active input channels, but does *not* save the data to disk. Idle mode is designed to allow the user to monitor the laser spectrometer while awaiting a hardware or software trigger ('T' or 't' from the keyboard). Once a trigger is received the program switches to run mode; the trigger time is noted and the data are now saved to a virtual disk whenever the data arrays are filled. After writing to the virtual disk, the arrays are re-initialized and the data collection resumed. Dumping data to the virtual disk circumvents the limitations of the standard DOS 640 kB memory barrier without a significant loss of duty cycle. (OXY is restricted to conventional DOS real mode operation because the proprietary drivers supplied with the Analog Devices RTI-860 digitizer board will only operate in real mode.) Thus, the number of data arrays kept in memory determines, in part, how often data are written to the virtual disk and the amount of time required whenever the virtual disk is accessed. Data collection continues until either the virtual disk is filled or the user types <ALT>-F1. All of the data, including the file created on the virtual disk, are then written to the hard disk for permanent storage and OXY returns to the set-up menu.

OXY was written in turboPascal and compiled using version 7.0 of the Borland Pascal compiler. In addition, we wrote a customized data handling subroutine that is incorporated into the terminate-and-stay-resident program controlling the Analog Devices RTI-860 digitizer board. That subroutine, USCAN, is written in assembly language and was assembled using the Borland Turbo Assembler (v 3.2). UPROCOXY.OBJ is linked to object modules and libraries supplied by Analog Devices. The linker is Borland TLINK (v 5.1). The resulting terminate-and-stay-resident program, PASLOADO, must be invoked prior to running OXY and requires a set-up data file, CONF.DAT. We include a batch file, OXY.BAT, which can be invoked from the DOS prompt and runs the programs in the required order.

6. CONCLUSIONS AND RECOMMENDATIONS

Most of the technical objectives of this program were met. A multi-channel diode laser/fiber optic system capable of measuring O_2 concentrations, gas temperature, and flow velocity in high temperature, high speed wind tunnel flows was designed, constructed, and tested. The fundamental spectroscopic parameters required for quantitative measurements using this system were measured in laboratory studies. An extensive set of experiments in a fuel-lean premixed flat flame was performed in order to evaluate the accuracy of temperature and concentration measurements based on the diode laser absorption technique. These experiments permitted evaluation of the effects of a nonuniform temperature profile on concentration measurements and suggested the need for careful selection of the O_2 absorption lines used, based on the particular characteristics of the system under study. Difficulties encountered with the scheduling and availability of wind tunnel facilities at NASA Langley precluded our testing the system on a wind tunnel during this phase of the work, however, the system delivered to NASA is ready for use in this application.

Several areas can be identified where design improvements might improve the sensitivity and reliability of the system. These areas include:

i) Laser power and reliability. Important advances are continually being made in the fabrication of near-infrared and visible diode lasers. These advances are likely eventually to lead to the availability of higher power single frequency lasers in the 760 nm region. In the present study, we found that the available laser power, particularly after introduction into an optical fiber system, limited the number of optical channels that we could successfully design into the system. Also, the spectroscopically useful lifetime of the diode lasers was limited, as tuning characteristics would change over time so that a particular spectral interval containing the desired O_2 absorption lines might eventually become inaccessible. An interim solution to this problem may be the use of short external cavity designs, such as those due to Cassidy.[22] This design stabilizes the single mode spectral tuning parameters of the laser while still permitting the fast wavelength modulation techniques that are required for high sensitivity.

ii) Multi-channel system. The fiber optic-based multichannel system developed in this program was the source of much trial and error in design. Most of these difficulties arose because of the propensity of the fiber system to induce unwanted etalon effects that limited measurement sensitivity. The need for careful angling of optical surfaces relative to the optical axis has been described in this report. We believe that direct fiber pigtailing of the laser, with an integral optical isolator, may alleviate many of the problems we encountered. This technology is routine in the InGaAsP diode lasers used at longer near-IR wavelengths for fiber optic communications, but it is rarely used with the shorter wavelength lasers designed primarily for optoelectronic applications. Our attempts to develop such a design, utilizing the fiber pigtailing services of two outside sources, did not yield positive results during this program, but we believe that further persistence is justified.

7. REFERENCES

1. J. J. Singh, W. T. Davis, and R. L. Puster, "Proposed Fast-Response Oxygen Monitoring and Control System for the Langley 8-Foot High-Temperature Tunnel," NASA TP-2218 (1983).
2. M. P. Lee, P. H. Paul, and R. K. Hanson, "Laser-Fluorescence Imaging of O_2 in Combustion Using an ArF Laser," Opt. Lett.**11**, 7 (1986).
3. J. E. M. Goldsmith and R. J. M. Anderson, "Laser-Induced Fluorescence Spectroscopy and Imaging of Molecular Oxygen in Flames," Opt. Lett. **11**, 67 (1986).
4. D. E. Burch and D. A. Gryvnak, "Strengths, Widths, and Shapes of the Oxygen Lines Near 13,100 cm^{-1} (7620 Å)," Appl. Opt. **8**, 1493 (1969).
5. J. Miller, R. Boese, and L. Giver, "Intensity Measurements and Rotational Intensity Distribution for the Oxygen A-Band," J. Quant. Spectrosc. Radiat. Transfer **9**, 1507 (1969).
6. K. J. Ritter and T. D. Wilkerson, "High Resolution Spectroscopy of the Oxygen *A* Band," J. Mol. Spectrosc. **121**, 1 (1987).
7. L. S. Rothman, R. R. Gamache, R. H. Tipping, C. P. Rinsland, M. A. H. Smith, D. C. Benner, V. Malathy Devi, J.-M. Flaud, C. Camy-Peyret, A. Perrin, A. Goldman, S. T. Massie, L. R. Brown, and R. A. Toth, "The HITRAN Molecular Database: Editions of 1991 and 1992," **48**, 469 (1992).
8. K. J. Ritter, "A High Resolution Spectroscopic Study of Absorption Line Profiles in the A-Band of Molecular Oxygen," Ph. D. Dissertation, University of Maryland, 1986.
9. G. Herzberg, Molecular Spectra and Molecular Structure II. Spectra of Diatomic Molecules (Van Nostrand Reinhold, New York, 1950).
10. J. Silver, "Frequency-Modulation Spectroscopy for Trace Species Detection: Theory and Comparison Among Experimental Methods," Appl. Opt. **31**, 707 (1992).
11. D. S. Bomse, A. C. Stanton, and J. A. Silver, "Frequency Modulation and Wavelength Modulation Spectroscopies: Comparison of Experimental Methods Using a Lead-Salt Diode Laser," Appl. Opt. **31**, 718 (1992).
12. J. Reid, M. El-Sherbiny, B. K. Garside, and E. A. Ballik, "Sensitivity Limits of a Tunable Diode Laser Spectrometer, with Application to the Detection of NO_2 at the 100-ppt Level," Appl. Opt. **19**, 3349 (1980).
13. D. E. Cooper and R. E. Warren, "Two=Tone Heterodyne Spectroscopy with Diode Lasers: Theory of Line Shapes and Experimental Results," J. Opt. Soc. Am. B **4**, 470 (1987).
14. D. Herriott, H. Kogelnik, and R. Kompfner, "Off-Axis Paths in Spherical Mirror Interferometers," Appl. Opt. **3**, 523 (1964).
15. P. L. Varghese and R. K. Hanson, "Collisional Narrowing Effects on Spectral Line Shapes Measured at High Resolution," Appl. Opt. **23**, 2376 (1984).
16. K. C. Smyth, J. H. Miller, R. C. Dorfman, W. G. Mallard, and R. J. Santoro, "Soot Inception in a Methane/Air Diffusion Flame as Characterized by Detailed Species Profiles," Combust. and Flame **62**, 157 (1985), and references therein.
17. E. R. G. Eckert and R. M. Drake, Jr., *Analysis of Heat and Mass Transfer* (McGraw Hill, New York, 1972), p. 414.
18. D. Bradley and A. Entwistle, "Determination of the Emissivity of Small Diameter Platinum - 10% Rhodium Wires in the Temperature Range 600 -1450 °C," Brit. J. Appl. Phys. **12**, 708 (1961).
19. J. H. Kent, "A Noncatalytic Coating for Platinum-Rhodium Thermocouples," Combust. and Flame **14**, 279 (1970), and references therein.

20. J. R. Veale and T. F. Gallagher, "Spectroscopic Monitoring of O_2", Final Report, Dept. of Physics, University of Virginia, (1992).

21. D. B. Oh, D. S. Bomse and A. C. Stanton, "Quantitative Measurement of O_2 in Laboratory Flames Using Near-IR Diode Lasers", 1991 OSA Annual Meeting, San Jose, CA, (1991).

22. D. Bruce and D. T. Cassidy, "Detection of Oxygen Using Short External Cavity GaAs Semiconductor Diode Lasers," Appl. Opt. **29**, 1327 (1990).

APPENDIX: INSTRUMENT MANUAL

Nonintrusive Fast Response Oxygen Monitoring System
for High Temperature Flows

TABLE OF CONTENTS

1. INTRODUCTION

This manual, which is Appendix A of the Phase II SBIR final report, explains the physical layout and the operating procedures for the Southwest Sciences multichannel fiber optic oxygen monitor. The main body of the final report details the basic theory of wavelength modulation spectroscopy using near-infrared diode lasers, instrument design criteria, and the performance specifications of the instrument. Experimental results for temperature and concentration measurements of O_2 in premixed flat flames and estimates of detection sensitivity are also presented in the main body of the final report.

The fiber optic oxygen monitor uses optical absorption to measure temperature, oxygen concentration, and velocity in high temperature fast flows. Sections 2 and 3 of this manual describe the electronic and optical components that make up the instrument. Section 4 describes the setup procedure for the instrument while Section 5 details instrument operation including suggestions on how to optimize detection sensitivity. Section 6 describes the procedure for retrieving and analyzing the acquired data from oxygen measurements in high temperature fast flows. Section 7 provides a list of suppliers for the various components used in the instrument.

Most questions regarding routine operation of the instrument are discussed in Section 5.

2. ELECTRONIC COMPONENTS

Laser Diode and Control Electronics

The Mitsubishi ML 4405 diode laser has a manufacturer-specified wavelength of 750 ±10 nm with nominal output power of 3 mW at room temperature and is available from several suppliers. Since the oxygen sensor is based on monitoring a pair of absorption features (RQ(23,24) at 13163.7871 cm^{-1} and RQ(33,34) at 13164.1963 cm^{-1} in the O_2 A ← X (0,0) band), the instrument requires laser diodes that will continuously tune over the selected wavelength region. *However, obtaining laser diodes preselected for assured tuning across the wavelength range of interest is not generally possible.* The typical procedure has been to purchase several diode lasers from those suppliers (e.g. ILX Lightwave) who are willing to hand pick diode lasers with room temperature wavelengths close to 760 nm. The tuning behavior of these lasers is then characterized with a wavemeter (Burleigh W-100).

The laser chip is housed in a hermetically sealed TO-5 can, but it is quite susceptible to damage due to static discharge. Therefore, proper grounding of the laser handler is essential to enable prolonged operation of the laser diode. Grounding cables are provided to connect the laser diode handler and the laser housing with the chassis ground port of the diode laser current controller. We recommend that the diode lasers be kept in their factory-provided envelopes with conductive inner surfaces when not in use.

The diode laser is housed in a commercial housing (ILX LDM-4412) with 9-pin subminiature D-connectors for the cables from the current and temperature controllers. In addition, a multi-element collimating lens assembly in front of the laser diode allows fine control of the focusing of the laser output. Detailed schematics of this commercial laser housing are available in the ILX manual.

The diode laser is connected to the current source by a 3-pin Teflon socket which in turn connects to a 9 pin subminiature D-connector port. The connector pins of the diode laser are matched by the hole pattern of the 3-pin Teflon socket. The laser diode is installed in a clearance hole of an aluminum plate, which is in thermal contact with a pair of thermoelectric coolers. The temperature controller is connected to the thermoelectric coolers and a thermistor (imbedded in the aluminum plate) by a second 9-pin subminiature D-connector port. These connections, which are standard for this laser housing, are described in greater detail in the LDM-4412 manual.

The output wavelength of the diode laser varies with either the temperature or the applied current level, with generally finer control to be had with variation of the current setting. The oxygen sensor is designed to operate at fixed diode laser temperature with a train of current ramps that scan the laser wavelength repetitively over the absorption feature of interest. The temperature of the diode laser mounting plate is monitored with an imbedded thermistor, which is read by the diode laser temperature controller (ILX LDT-5910B). This controller also powers the two thermoelectric coolers that are in thermal contact with the laser mounting plate and adjusts the temperature of the plate to maintain a constant laser temperature. The temperature of the diode laser mounting plate can be set and regulated within ±0.05 °C of the set temperature.

The thermistor (Dale Model 1T1002-5) is provided by ILX Lightwave Corporation along with the diode laser housing. A calibration table showing temperature vs. resistance is provided along with the three constants that are used in the Steinhart-Hart equation for conversion of resistance to temperature by the temperature controller. The Steinhart-Hart equation is $1/T = (C_1 \times 10^{-3}) + (C_2 \times 10^{-4})(\ln R) + (C_3 \times 10^{-7})(\ln R)^3$. The thermistor installed in the diode laser mounting plate at time of delivery has part # DL 890232, and $C_1 = 1.107$, $C_2 = 2.365$, and $C_3 = 0.807$. These constants are saved in the non-volatile memory of the temperature controller. The procedure of displaying or altering these constants is detailed in the temperature controller user manual.

After the ILX LDT 5910B temperature controller is turned on, the desired temperature set point can be established by pressing the "SET TEMP" button and then turning the main control knob. When the "LOCK" button is on, the temperature set point cannot be changed. When the "OUTPUT" switch is pressed, the temperature control function is enabled. Further detailed description of the front panel switches can be found in the ILX LDT-5910B instruction manual.

On the rear panel of the temperature controller, the "SELECT SENSOR" switch at the time of instrument delivery was set at 100 μA for operation in the -10 to 100 °C temperature range using the Dale 10 kΩ thermistor. This setting can be switched to 10 μA for -50 to 40 °C operation, if necessary. The temperature controller is connected to the diode laser housing by a 15-pin-to-9-pin connector cable. Further information on different temperature sensing applications can be found in the temperature controller instruction manual.

The 15pin-to-9pin output cable from the LDT 5910B utilizes TE Module (+) and (-) connectors (pins 1, 2 and 3, 4, respectively) and sensor (+) and (-) connectors (pins 7 and 8, respectively) to supply driving current to the thermoelectric coolers and to read the thermistor. This cable is connected to the 9-pin socket on the LDM-4412 laser mount.

The laser diode current is supplied by an ILX ultra low noise current source (Model LDX-3620). This unit provides battery powered operation with < 850 nA noise and ripple for 5 Hz - 10 MHz bandwidth of operation. For operation of the ML4405 diode lasers, the current range is set at 0 - 200 mA with a transfer function of 100 mA/V between the external modulation input and the output current. Therefore, we would use 100 mV of voltage ramp to obtain 10 mA in current ramp.

The DC power range and the powering of the current source are selected with a key switch on the lower left-hand corner of the front panel. The "OUTPUT ON/OFF" push button on the lower right corner enables the current supply to the laser diode. The LCD display turns on when the power is "ON" though the output switch is turned "OFF", thereby allowing adjustment of the current setting before powering the laser. The "LIMIT CURRENT ADJUSTMENT" knob limits the maximum current supplied to the laser diode, which is set at ~ 73 mA for the Mitsubishi ML 4405 diode lasers. The "MODULATION MODE SELECT" switch is set at "EXT DC", which allows eternal modulation from DC to 1 MHz. The voltage ramp (which is converted to a current ramp by the 100 mA/V transfer function), with 50 kHz sinusoidal modulation, is connected to the "EXTERNAL MODULATION INPUT" by a BNC T-connector. The current level can be changed by two "OUTPUT ADJUST" knobs allowing coarse and fine control.

On the rear panel of the LDX 3620, the "OUTPUT" 9-pin connector allows a subminiature D-connector to mate and supply current to the laser diode in the housing. The "BANDWIDTH SELECTOR" switch is set at "HIGH" for the 50 kHz modulation frequency. The "AC POWER ON/OFF" switch is turned on when battery recharging is needed.

On the 9-pin output cable, only the current output (+) and (-) connectors (pins 8, 9 and 4, 5, respectively) are used to connect the current source to the laser diode with a cable connection to the 9-pin connector on the diode laser housing. More detailed description of the current source can be found in the ILX LDX-3620 instruction manual.

In order to characterize the laser diode tuning behavior, the laser temperature would be set at a given temperature (preferably near room temperature) while the current setting is varied and the laser output wavelength is monitored with a wavemeter. If no satisfactory tuning mode is located, the laser temperature is changed and the process is repeated.

The typical operating temperature of the Mitsubishi ML 4405 laser diode in this application is between about 18 °C to 30 °C depending on the tuning characteristic of each laser. Since higher operating temperatures increase the laser threshold current and reduce the output power of the laser at a given current setting, we prefer to work with those diode lasers that operate at the desired wavelength near room temperature (or cooler if possible) and a current setting of 60 to 65 mA.

Detection Electronics

The 50 kHz laser current modulation is provided by a Wavetek 2 MHz function generator. The frequency is set by a combination of variable and fixed gain knobs. The 50 kHz sinusoidal waveform from the "Func Out" BNC connector is sent to the "External Modulation" port of the diode laser current source and is coupled by a 15 μf coupling capacitor. The amplitude of the modulation waveform is adjusted using "Amplitude" adjust. For the oxygen monitor, 20 dB "Attenuation" is used with the amplitude adjustment knob for optimum wavelength modulation.

The synchronous 50 kHz TTL output is sent to the phase shift/doubler box. The inner layout of the box is shown in Fig. A-1. The Evans Electronics phase adjuster/doubler card (Model 4114) allows fine and coarse phase adjustment and generation of the second harmonic frequency at 100 kHz. The front panel of the phase shifter/doubler has a 10 kΩ pot for fine control and two toggle switches for 90° and 180° phase shift of the 100 kHz waveform.

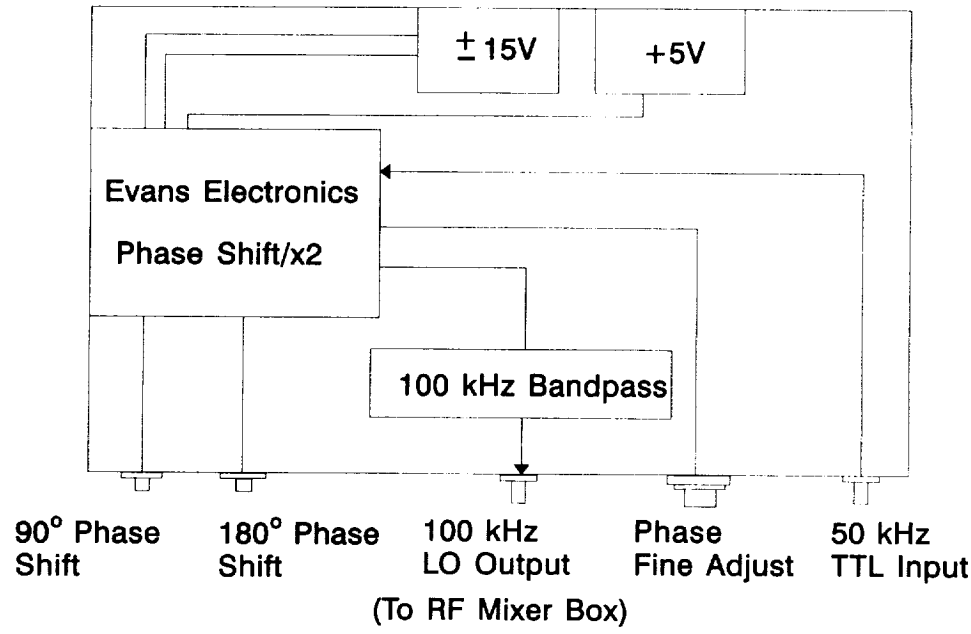

Figure A-1. Phase-shift/frequency doubler box layout.

Figure A-2 shows the pin assignments of the Evans Electronics card. *The card is installed upside down so that the component side faces down while the soldered side faces the top panel of the enclosure.* The resulting 100 kHz sine wave is sent to the rf mixer box for 2f detection.

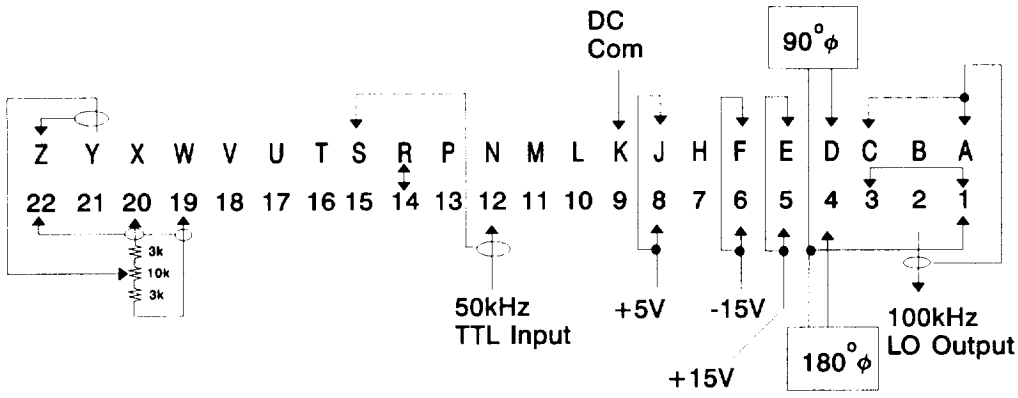

Figure A-2. Evans Electronics phase shift card pin assignments.

The Si photodiode (Centronics Model OSD-5T), which is mounted on a 3-pin detector socket of the Analog Modules detector/preamplifier box, monitors the laser beam. It has an active area of 5 mm^2, a responsivity of 0.55 amp/watt, and a 7 ns rise time.

An Analog Modules detector/preamplifier (Model 310-46) provides AC and DC outputs for simultaneous $2f$ detection of absorbance and laser beam intensity (I_0) monitoring. Detailed schematics of the detector/preamplifier are not available due to the manufacturer's refusal to supply them, but a general schematic drawing is shown in Fig. A-3.

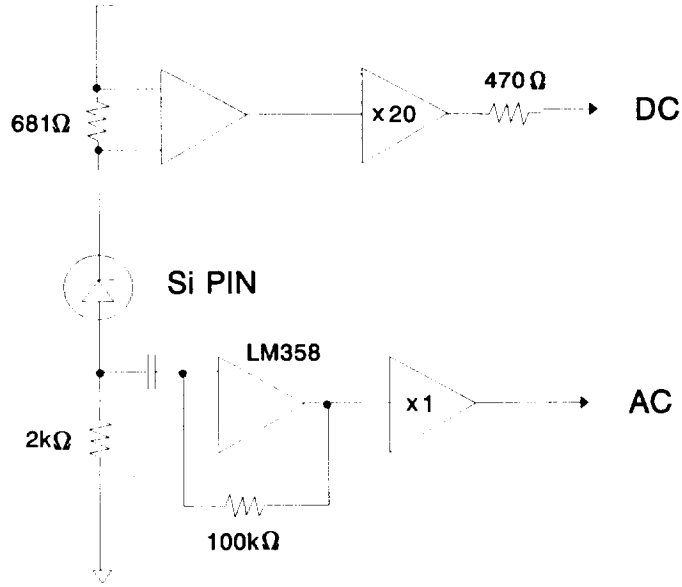

Figure A-3. Schematic of the Analog Modules 310-46 detector/preamplifier.

The AC output provides a total gain of 100 kV/A with 0.678 pA/$\sqrt{\text{Hz}}$ current noise, while the DC output provides a 1 kHz low pass filtered signal with total gain of 13.6 kV/A. Voltage input of ±15 volts is supplied to the detector/preamplifier through connector pins. The detector/preamplifiers are enabled by switching on the power supply.

The Pacific Instruments amplifier/filter units provide the needed signal conditioning before digitization and storage. The rack housing (Model R16BC) provides the necessary power to the 8 amplifier/filter modules (Model 3100). The DC output from the detector/preamplifier is amplified and filtered before the analog divider circuit for normalizing the $2f$ absorption signal. The AC output from the detector/preamplifier, after demodulation at $2f$ in the rf mixer, is amplified and low pass filtered before it is sent to the analog divider for normalization. All input and output BNC connectors located in the rear panel are clearly labeled. The front panel of the amplifier/filter module is also clearly labeled for variable gain and low pass filter settings. More detailed information can be found in the Pacific Instruments user manual.

As mentioned above, the AC output from the Analog Modules detector/preamplifier is sent to the rf mixer box for $2f$ demodulation. Fig. A-4 shows a block diagram of the rf mixer box. The AC signal from the detector/preamplifier, after entering the box by BNC connection on the lower right hand side of the front panel, is high pass filtered (TTE HE-1182-60K-50-6140) at 60 kHz to block out $1f$ and pass $2f$ and then sent to the "R" (radio frequency) port of the rf mixer (Mini-Circuits ZAD-8). The 100 kHz phase adjustable sine wave is introduced into the box through a BNC connector marked "LO" on the rear panel. It is then amplified (Analog Modules Model 351-2-B-50-NI) and band pass filtered at 100 kHz (TTE Model Q70-100K-30K-50/50-720B) before it is split into 8 outputs by an 8-way rf splitter (Mini-Circuits Model ZFSC-8). The output is fed to the "L" (local oscillator) port of the rf mixer for $2f$ demodulation. The signal out of the "I" port is sent to the Pacific Instruments amplifier/filter module for signal conditioning.

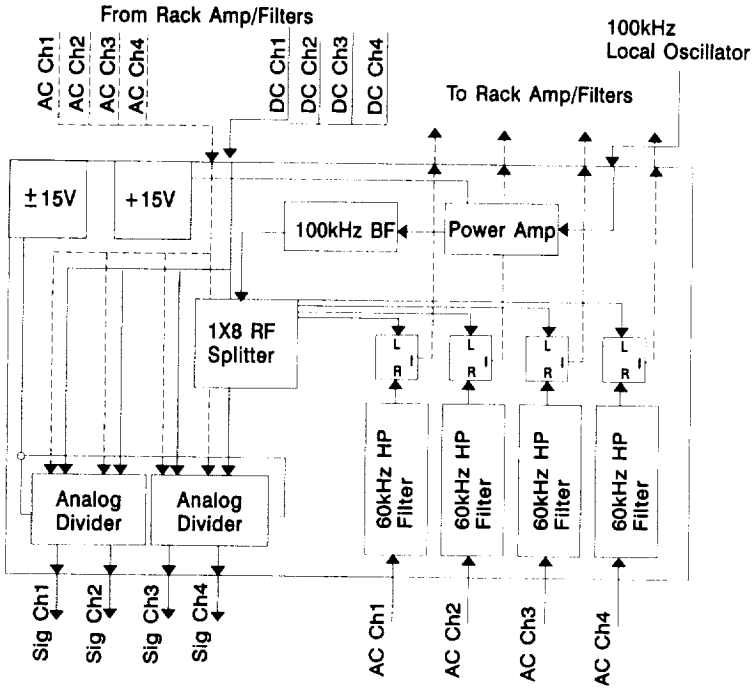

Figure A-4. Block diagram of the rf mixer box.

The rf mixer box also houses two analog divider boxes, where each box contains two analog divider chips (Analog Devices Model AD734) for normalization of the $2f$ signals by the corresponding DC signals (I_0). The wiring diagram of the analog divider chip is shown in Fig. A-5. The AC and DC signals, properly conditioned by the Pacific Instruments amplifier/filters are fed back into the rf mixer box via BNC connectors in the rear panel. The divider box requires ±15 volts. The outputs from the analog dividers are fed to BNC connectors on the lower left-hand side of the front panel. The normalized signal outputs are connected to the A/D BNC connector panel for digitization and storage.

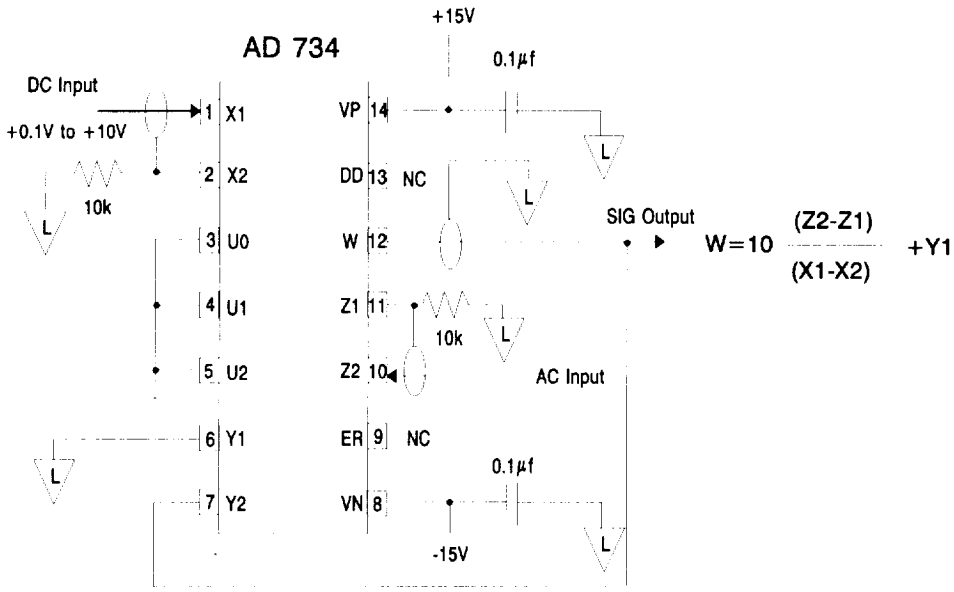

Figure A-5. Wiring diagram of the analog divider chips.

The A/D BNC panel is connected to the A/D board (Analog Devices Model RTI-860), which is housed in the Northgate computer, by the 50-pin ribbon cable. The waveform synthesizer board (Qua-Tech WSB-10) installed in the Northgate computer has BNC outputs for the programmed waveform, trigger, and the tracer. The output assignments are shown in Fig. A-6. The synthesized waveform output is fed to the external modulation input port of the laser current source for repetitive wavelength sweeps. The trigger output is used to trigger the oscilloscope for real time viewing of the $2f$ absorption feature, and the pacer output is fed to the pacer out port of the A/D BNC panel.

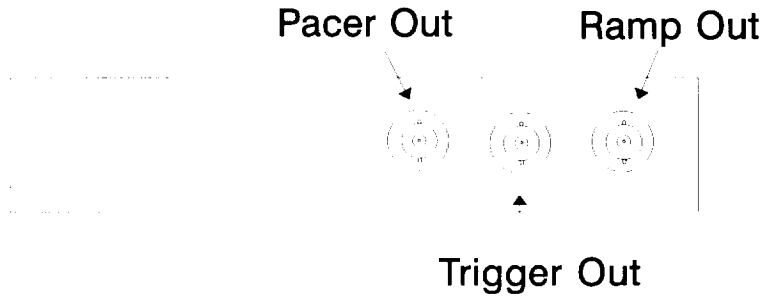

Figure A-6. Assignment of the WSB-10 board BNC outputs.

Data acquisition and storage, using the Northgate 386 computer, are described in Section 5.3 of the main body of the final report. The data acquisition program can be triggered to start data acquisition either by a keyboard command (by pressing "T") or by sending a trigger pulse (+2.5 Volts or greater, 100 ns or longer) to an 8-bit A/D board (Keithley Metrabyte Model DAS-4). A BNC cable-to-36-pin connector is provided for the external trigger pulse.

3. OPTICAL COMPONENTS

The light output from the diode laser is collimated and focused with a 3-element lens assembly (Rodenstock Model 830.1403.169.000), which is mounted on a threaded brass adapter of the diode laser housing for fine control. The laser beam is coupled into the single mode fiber (3M FS-SN-4221) by a collimating GRIN lens, which is mounted on an XY-tilt/adjust stage (Newport Model F-915).

To reduce the feedback noise from the back-scattered laser beam off the GRIN lens/fiber assembly, an optical isolator (Isowave Model I-80-T4) is mounted between the diode laser and the input GRIN lens. Based on the Faraday rotation effect, the polarization of the linearly polarized input beam is rotated by 45° as it passes through the isolator while the reflected beam is rotated by another 45° to be perpendicular to the input linear polarizer. Because of interferences observed between the input and output sides of the isolator surfaces, the input face was custom tilted by 2°. However, careful tilt adjustment is needed to minimize etalon effects in the signal baseline.

The laser beam is coupled into the single mode fiber by a GRIN lens attached to the tip of the fiber. The GRIN lens is fused onto the tip of the single mode fiber to reduce back reflection from the GRIN lens-to-fiber junction. The GRIN lens is angle-polished at a 2° angle and AR coated to reduce the etalon between the GRIN lens and the optical isolator. A removable purge box can be installed over the laser beam-to-fiber optic coupling assembly to purge background oxygen.

The single mode fiber (3M Model FS-SN-4221) used to carry the laser beam was manufactured by 3M Specialty Fibers Division. It contains a 4.7 μm diameter fiber core, 125 μm diameter cladding, and a reinforced jacket outer shell to make the fiber rugged. The light attenuation at 760 nm is 4.5 dB/km, causing the laser power to drop ~4% after 100 feet of fiber used to transport the light to the detection region.

The laser beam, after 100 feet of fiber optic cable, is split into 4 outputs with a 1×4 fiber optic splitter (Amphenol 945-999-1611). The four outputs from the fiber optic are collimated with a GRIN lens (OZ Optics, Ltd. Model LPC-01-760-5/125-0.4-1.8-45). The lens provides a 0.4 mm diameter beam with a divergence of 1.8 mrad. The surface of the GRIN lens was polished at 2° and AR coated to minimize the etalon effects within the GRIN lens. Because of the angle polish on the GRIN lens surface, the laser beam exiting from the GRIN lens has a small angular deviation from the GRIN lens axis. Therefore, the GRIN lens adapter to the wind tunnel facility was designed to compensate for the deviation.

Between optical components where the fiber optic cables are not continuous, the two fiber ends must be joined. One method is to attach a connector assembly on each fiber end and then join the fibers with an adapter. During initial development, ST-type connectors were used to make such connections. However, consistency in fiber-to-fiber coupling efficiency was lacking in such connectors. Therefore, all the fiber joints were replaced with fusion splicing where the fiber ends are permanently joined. Although some convenience in sensor setup may have been lost, the laser power level at each fiber output is now determined by the input coupling efficiency alone.

The solid etalon assembly is used to generate accurate frequency markers during flow velocity measurements in the wind tunnel. A schematic diagram of the etalon assembly is shown in Fig. A-7. The collimated laser beam from the output GRIN lens is first expanded with a telescope, then it is sent through a 1" diameter solid etalon (CVI Model ET-25.4-50.0-760-90, 2.04 GHz FSR). Finally, the beam is focused onto a Si photodiode mounted on an Analog Modules detector/preamplifier. The AC output from the detector is then processed for $2f$ detection and etalon fringes are recovered. For ease of visualizing the interference ring pattern during initial alignment, a He-Ne tracer beam may be used.

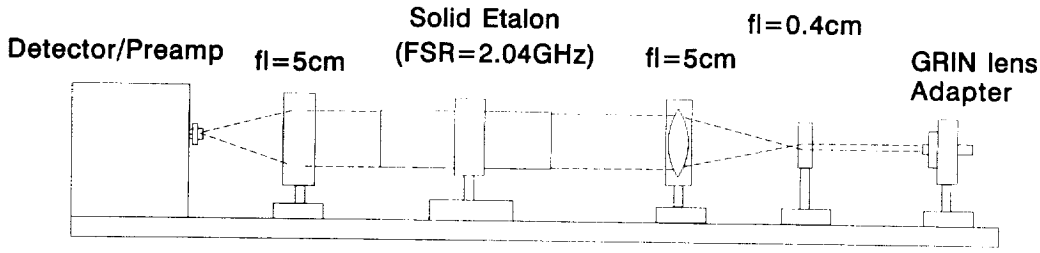

Figure A-7. Schematic drawing of the solid etalon assembly.

The optical alignment of the other detection channels may be verified or further optimized by monitoring the DC output from each detector/preamplifier. The wind tunnel fiber adapter holds the transmitting GRIN lenses and the receiving Si photodiode detectors in their positions during the wind tunnel measurement. Although each detection port is prealigned, the GRIN lenses should be rotated within their holders to ensure optimum alignment.

4. SETUP PROCEDURE

This section describes the instrument setup procedure assuming each component is disassembled from one another. Fig. A-8 shows the diagram of the assembled instrument.

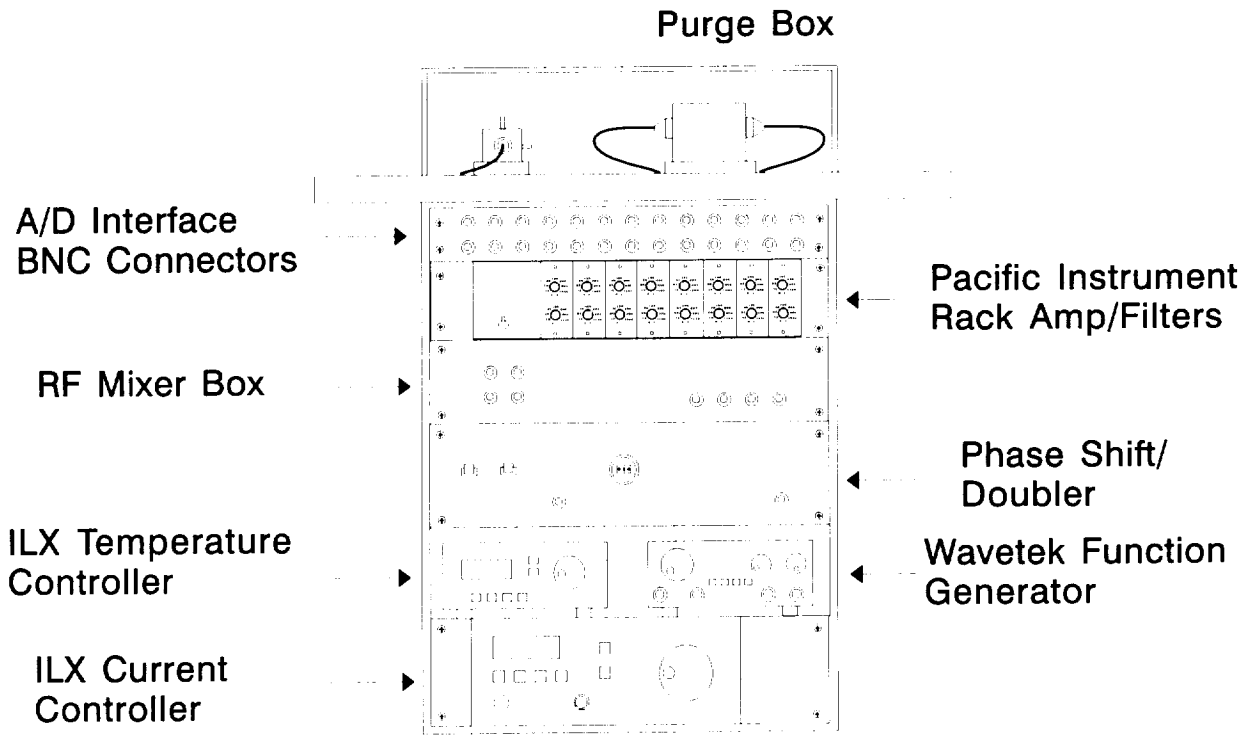

Figure A-8. The assembled oxygen sensor.

The installation begins with the optical setup of the laser beam-to-fiber coupling stage (see Fig. 4.1 of the main report for the schematic diagram). The laser diode housing is connected to the laser current source and the laser temperature controller by 9-pin D-sub connectors. The two flat beam steering mirrors are positioned near two corners of a long end of the rectangular area defined with foam strips on top of the miniature breadboard. The XY-tilt/adjust stage, which houses the GRIN input lens, is set on the same side as the laser housing, which is the opposite long side of the rectangle. The optical isolator is mounted on an XY translation stage, and it is positioned near the GRIN lens. The laser beam should be collimated but gently focusing as it enters the GRIN lens. The idea is to match the 0.3 NA of the input GRIN lens for optimum coupling efficiency. Finally, the linearly polarized diode laser beam needs to be matched to the input polarization direction of the optical isolator for maximum transmission.

The breadboard containing the input coupling optics can be set onto the steel rack. Next, each rack component is installed at the appropriate location. The current source, temperature controller, and function generator are placed on the bottom space of the rack.

To optimize the laser beam-to-fiber coupling efficiency, one may wish to bring the Si photodiode detector close to the GRIN collimating output lens. Make necessary adjustments with the mirrors and/or XY fine adjustments built into the diode laser housing to bring the laser beam clear through the optical isolator and centered on the GRIN lens mounting hole of the XY-tilt/adjust stage. While monitoring the DC output from the detector on an oscilloscope, a systematic adjustment of the XY tilt of the GRIN lens mount should be made. *This is often the most time consuming, but probably the most important, step in setting up the instrument.*

The 50-pin ribbon connector from the BNC panel should be connected to the RTI-860 board in the Northgate computer. The waveform output from the WSB-10 board should be connected to the laser current source via the voltage divider. The trigger and tracer outputs from the WSB-10 board are connected to the trigger port of an oscilloscope and the tracer out port of the BNC panel, respectively. The "Func Out" port from the Wavetek function generator should be combined with the voltage ramp output from the WSB-10 board.

The TTL output from the 50 kHz function generator should be connected to the 50 kHz input connector on the back of the phase shifter box. The resulting 100 kHz sine wave from the front panel of the phase shifter box is fed to the "LO Input" BNC located on the rear panel of the rf mixer box.

The detector/preamplifier DC output is sent to the Pacific Instruments amplifier/filter module, and then it is sent back to the "DC In" BNC connector on the rear panel of the rf mixer box. The AC output from the detector /preamplifier is sent to the "Sig In" BNC connectors on the front panel of the rf mixer box. The "AC Out" BNC on the rear panel of the rf mixer is connected to the Pacific Instruments amplifier/filter and then back to the "AC In" BNC on the rear of the rf mixer box. The "Sig Out" from the front panel of the rf mixer box is connected to the A/D BNC panel for digitization. All these ports are marked with corresponding channel numbers, and consistent adherence to the channel number will prevent any confusion. In this section, we have assumed that internal BNC cables inside the rf mixer box have not been disturbed. If the BNC cables inside the box need to be reconnected, Fig. A-4 should be consulted for further details.

Use of the solid etalon assembly is straightforward when Fig. A-7 is consulted.

Finally, Table 1 summarizes the BNC coaxial cable connections that need to be made externally between components.

Table 1 - BNC Connections

From							To
Detector DC	-cable->	rack amp/filter	-cable->	rf Mixer DC In			
Detector AC	-cable->	rf Mixer Sig In	rf Mixer AC Out	-cable->	Rack amp/filter	-cable->	rf Mixer AC In
rf Mixer Sig Out	-cable->	A/D Panel					
Wavetek Func Out	-cable->	LDX3620 Ext Mod					
Wavetek TTL Out	-cable->	ϕ Control LO In	LO Out	-cable->	rf Mixer LO In		
WSB-10 Func Out	-cable->	Voltage Divider	-cable->	LDX3620 Ext Mod			
WSB-10 Tracer Out	-cable->	A/D Panel					

5. OPERATION

The oxygen monitor, when set up and aligned with the procedures outlined in Section 4, should be ready for operation. Begin by powering up each component, including the Northgate computer. The laser temperature controller (ILX LDT-5910B) and laser current source (ILX LDX-3620) can be turned on, but the output should be disabled for now. Next, enable the temperature controller output and verify that the laser temperature stabilizes to the set point temperature. Take the synthesized ramp output from the WSB-10 board, which is connected to the voltage divider for adjustment, to an oscilloscope and verify that the ramp voltage does not exceed the maximum laser diode current limit. The voltage to current transfer function is 100 mA/V for the 0-200 mA output setting, and the current setting on the Mitsubishi ML 4405 diode laser should not exceed 70 mA. The ramp can be combined with the 50 kHz sine wave and connected to the "Ext Mod Input" port of the current source.

Next, take the $2f$ signal (AC output) and the corresponding DC output from the Pacific Instruments amplifier/filter units and display them on the scope. By enabling the current output of the diode laser current source, the laser will be powered up and the DC signal will appear on the scope. If there is oxygen along the laser beam path, some $2f$ absorption signal will be observed as well. At this point, the optical alignment of the laser-to-fiber can be checked again and optimized further if necessary. As the DC signal increases due to improvements in the laser-to-fiber coupling efficiency, the $2f$ absorption signal level will also increase. However, unwanted etalon fringe signals may also increase in amplitude as the optical alignment is changed . *It is important to strive for the optical alignment that produces the best signal-to-baseline noise ratio.*

After the laser-to-fiber alignment is checked and aligned for the optimum signal-to-baseline noise, the $2f$ signals from the different detectors should be monitored simultaneously while the modulation frequency is adjusted by ± 10 kHz from the 50 kHz center frequency. Each detection channel, which uses 60 kHz high pass filters to reject the $1f$ component and detect $2f$, may have somewhat different frequency transmission characteristics at the detected $2f$ frequency. We have found that a modulation frequency of about 40.5 kHz results in good $2f$ signal levels on all four channels. Once the modulation frequency is optimized by observing all 4 detection channels simultaneously, no further adjustment will be necessary in subsequent operation of the instrument.

The modulation depth (or index of modulation) is adjusted by changing the amplitude setting of the $1f$ sine wave from the "Func Out" port of the frequency generator. The optimum modulation depth is dependent on the line width of the absorption feature, and it thus depends on the sample pressure and temperature. The optimally modulated $2f$ signal exhibits no further increase in peak-to-trough level, but widening of the trough-to-trough separation upon further increases in modulation amplitude can be seen. Therefore, the observed $2f$ signal must be calibrated with a known absorbance after the modulation amplitude is optimized. Once a calibration is obtained for each detection channel, the $2f$ signal from subsequent measurements can be converted to absorbance. A measured path length of room air can be conveniently used for such calibrations.

The instrument is now ready to measure oxygen concentration, temperature, and flow velocity in the wind tunnel test facility. Data acquisition can be initiated by either a trigger pulse to the DAS-4 board in the computer or by the keyboard command. Further description of the data acquisition software, including available options, can be found in Section 5.3 of the main portion of the final report.

The acquired data, which are saved on the hard drive of the Northgate computer, may be retrieved and analyzed using the data analysis routine supplied. Section 6 of this User Manual discusses the data analysis software, including its operation and built-in features.

The procedure of powering down the instrument is in reverse order of the powering up sequence. The diode laser current output should be disabled before any other actions are taken. The temperature

controller output may be disabled, and then the rest of the components may be powered down. The battery inside the diode laser current supply can be recharged by switching on the "AC Power" button.

6. DATA ANALYSIS

The data files acquired and stored with the "OXY.EXE" program can be retrieved and displayed for further analysis using a program called "OXY.DAT". Written in the programming environment called "ASYST", this program allows the user to specify the data file, input channel, and the data array of interest. The program opens and retrieves the corresponding data, and then it displays the data as a spectral scan. In addition, the time marker that corresponds to the time that the data were acquired is displayed on the bottom of the spectral display in units of seconds. The procedure for running the "OXY.DAT" program as well as some of its features are outlined below.

First, data files saved by the "OXY.EXE" program should be located and copied to the hard drive directory called "ASY400". (It is presumed that the "OXY.DAT" program is saved in this same directory.) Next, type "ASYST" at the DOS prompt to enter into the "ASYST" programming environment. The "ASYST" logo and the message "Strike any keys to continue" will appear on the screen. Upon hitting any key, the ASYST prompt "OK" will appear. At this prompt, type "LOAD OXY.DAT". Dotted lines will appear and then the ASYST prompt "OK".

At this point the program is loaded and ready to run. Type "START.DATA" and the program will prompt with "ENTER DATA FILE NAME :". Now type the full data file name with the extension. For instance, the data file name 071693.001 stands for the first set of data acquired on July 16th, 1993. The program returns with the data file description (up to 64 characters) and the prompt "ENTER DATA CHANNEL NUMBER :" and then "ENTER DATA ARRAY NUMBER :". The data array is a 2-dimensional array with dimensions given by the number of input channels and the number of data bins per spectral scan. The data array number runs from 1 to the total number acquired, and it also signifies the time elapsed during the measurement sequence. Upon entering the data channel number and the data array number, the program retrieves the specified spectral data and displays the data on the screen. At the bottom of the screen, "TIME MARKER (IN UNITS OF SECONDS) IS = ××××.×××" will be displayed. The time marker can be used to assess the time elapsed from one data array to the next array. When one wishes to retrieve another spectral scan (i.e. different data channel number or array number), enter "GET.DATA" at the ASYST prompt "OK". After entering the data channel number and data array number, the newly retrieved data will be displayed on the screen along with the time marker information. If another data file (i.e. another extension of the same date or different date) is to be opened, type "START.DATA" upon the ASYST prompt "OK" and repeat the above procedure.

Whenever new data are retrieved and displayed on the screen, the displayed data segment is stored in a data array called "DAT1". Therefore, the previous data segment is replaced by the latest one. Sometimes, one may wish to save retrieved data and retrieve a second data set for comparison. There are three other data arrays of equal length called DAT2, DAT3, and DAT4 for such temporary storage purpose. For instance, typing in " DAT1 DAT2 := " at the ASYST prompt "OK" will copy the currently displayed data segment into the data array " DAT2 ".

If one wishes to print the spectral data displayed on the screen, type " SCREEN.PRINT " after the ASYST prompt "OK". The ASYST programming environment has many features and options geared toward scientific analysis, and a proficient programmer of ASYST will find many more options at his/her command (e.g. peak finding, data smoothing, etc.).

When data retrieval and analysis are complete, one can exit the ASYST programming environment by typing " BYE " at the ASYST prompt "OK".

7. LIST OF SUPPLIERS

1. Diode Laser (Mitsubishi Diode Laser ML4405)

   ILX Lightwave Corporation
   P. O. Box 6310
   Bozeman, MT 58771
   (406) 586-1244

2. Diode Laser Housing, Temperature and Current Controllers

   (Laser Housing Model ILX LDM-4412, Diode Laser Temperature Controller Model LDT-5910B, Current Controller Model ILX LDX-3620)

   ILX Lightwave Corporation
   P. O. Box 6310
   Bozeman, MT 58771
   (406) 586-1244

3. Function Generator (Wavetek Model 20)

   Wavetek San Diego, Inc.
   9045 Balboa Ave.
   San Diego, CA 92123
   (619) 279-2200

3. Optical Isolator (Isowave Model I-80-T4)

   Isowave
   64 Harding Ave.
   Dover, NJ 07801
   (201) 328-7000

4. Optical Isolator Mount Stage, Fiber Optic Holder, and Fiber Mode Scrambler (Newport Model 460A-XZ, Newport Model F-915, and Newport Model FM-1)

   Newport Corp.
   1791 Deere Ave.
   Irvine, CA 92714
   (714) 863-3144

5. Fused GRIN Input Collimating Lens

   Optomec Design Co.
   1580 Center Dr.
   Santa Fe, NM 87505
   (505) 471-6516

6. Instrument Amplifiers/Filters (Pacific Instruments Model 3100 (Amp/Filter), R16BC (Rack Power Source)

   Pacific Instruments
   215 Mason Circle
   Concord, CA 94520
   (415) 827-9010

7. Phase Control Card (Evans Model 4114 Phase Control Card with 50 kHz Bandpass filter)

   Evans Electronics
   P. O. Box 5055
   Berkeley, CA 94705
   (415) 653-3083

8. Photodiode (Si) Detector (Centronic Model OSD36-5T)

   Centronic Inc.
   E-O Division
   1829 DeHavilland Dr.
   Newbury Park, CA 91320
   (805)499-5902

9. Detector/Preamplifier (Analog Modules 310-46)

   Analog Modules, Inc.
   126 Baywood Avenue
   Longwood, FL 32750
   (407) 339-4356

10. Fiber Optic Cable (3M FS-SN-4221)

    3M Specialty Optical Fiber
    420 Frontage Rd.
    W. Heaven, CT 06516
    (203) 934-7961

11. 1 × 4 Fiber Optic Splitter (Amphenol Model 945-999-1611)

    Amphenol Corporation/ Fiber Optic Products
    1925A Ohio St.
    Lisle, IL 60532
    (708) 960-1010

12. Fiber Optic Collimator (OZ Optics Model LPC-01-760-5/125-0.4-1.8-45)

    OZ Optics Ltd.
    PO Box 11218, Station 'H'
    Nepean, Ontario K2H 7T9 Canada
    (613) 831-0981

13. Thermoelectric Cooler for Laser Heat Sink (Melcor CP 1.4-35-06L)

    Materials Electronic Products Corporation
    990 Spruce Street
    Trenton, NJ 08648
    (609) 393-4178

14. ASYST Programming Environment

    ASYST Software Technologies, Inc.
    100 Corporate Woods
    Rochester, NY 14623
    (716) 272-8211

15. A/D Board (Analog Devices Model RTI-860)

    Analog Devices, Inc.
    One Technology Way, P.O. Box 9106
    Norwood, MA 02061
    (617) 329-4700

16. Programmable Waveform Generator (Qua Tech Model WSB-10)

    Qua Tech, Inc.
    478 East Exchange St.
    Akron, OH 44304
    (216) 434-3154

17. External Trigger Board (Keithley Metrabyte DAS-4)

    Keithley Instruments, Inc.
    440 Myles Standish Blvd.
    Taunton, MA 02780
    (508) 880-3000

18. Computer (Northgate 386)

    Northgate Computer Systems
    Dept. EW
    P. O. Box 59175
    Minneapolis, MN 55459
    (800) 648-6051

19. RF Mixer (Mini-Circuits ZAD-8), and 8-Way RF Splitter (Mini-Circuits ZFSC-8)

    Mini-Circuits
    P.O. Box 350166
    Brooklyn, NY 11235
    (718) 934-4500

20. 60 kHz High Pass Filter (TTE HE1182-60K-50-6140), and 100 kHz Bandpass Filter (TTE Q70-100K-30K-50/50-720B)

    TTE Incorporated
    2251 Barry Ave.
    Los Angeles, CA 90064
    (310) 478-8224

21. Solid Etalon (CVI Model ET-25.4-50.0-760-90)

    CVI Corp.
    200 Dorado Pl., S.E.
    Albuquerque, NM 87123
    (505) 296-9541

REPORT DOCUMENTATION PAGE

Form Approved
OMB No. 0704-0188

1. AGENCY USE ONLY (*Leave blank*)	2. REPORT DATE	3. REPORT TYPE AND DATES COVERED
	October 1993	Contractor Report

4. TITLE AND SUBTITLE
Nonintrusive Fast Response Oxygen Monitoring System for High Temperature Flows

5. FUNDING NUMBERS
C NAS1-19097
WU 324-02-01

6. AUTHOR(S)
Daniel B. Oh and Alan C. Stanton

7. PERFORMING ORGANIZATION NAME(S) AND ADDRESS(ES)
Southwest Sciences, Inc.
1570 Pacheco St., Suite E-11
Santa Fe, NM 87501

8. PERFORMING ORGANIZATION REPORT NUMBER
NASA CR-4553

9. SPONSORING / MONITORING AGENCY NAME(S) AND ADDRESS(ES)
National Aeronautics and Space Administration
Langley Research Center
Hampton, VA 23681-0001

10. SPONSORING / MONITORING AGENCY REPORT NUMBER
NASA CR-4553

11. SUPPLEMENTARY NOTES
Langley Technical Monitor: Jag J. Singh
Final Report - Phase II

12a. DISTRIBUTION / AVAILABILITY STATEMENT
Unclassified-Unlimited

Subject Category 35

12b. DISTRIBUTION CODE

13. ABSTRACT (*Maximum 200 words*)

A new technique has been developed for nonintrusive insitu measurement of oxygen concentration, gas temperature, and flow velocity of the test media in hypersonic wind tunnels. It is based on absorption of near-infrared radiation from inexpensive GaA1As laser diodes used in optoelectronics industry. It is designed for simultaneous measurements along multiple lines of sight accessed by fiber optics. Molecular oxygen concentration is measured from the magnitude of absorption signals; rotational gas temperature from this intensity ratio of two oxygen absorption lines; and the flow velocity from the Doppler shift of the absorption line positions. This report describes the results of an extensive series of tests of the prototype instrument in laboratory flames, emphasizing assessment of the instruments capabilities for quantitative measurement of 0_2 concentration (mole fraction) and gas temperature.

14. SUBJECT TERMS	15. NUMBER OF PAGES
Hypersonic vehicle development; Near-IR diode lasers; High frequency wavelength modulation spectroscopy; Spectroscopic measurements of temperature and concentration of 0_2 in pre-mixed flat flames	68
	16. PRICE CODE: A04

17. SECURITY CLASSIFICATION OF REPORT	18. SECURITY CLASSIFICATION OF THIS PAGE	19. SECURITY CLASSIFICATION OF ABSTRACT	20. LIMITATION OF ABSTRACT
Unclassified	Unclassified		